USACERL Technical Report EC-93/02
May 1993

US Army Corps
of Engineers
Construction Engineering
Research Laboratories

Sound Exposure Level Prediction for Impulse Sound Sources Above Variable Terrain

by
Hong C. Zhuang
Leslie J. Benson
Michael J. White

The influence of the ground surface makes it difficult to calculate the propagation of impulse noise from Army-type blasts such as that produced by heavy-weapons fire on training ranges. This study developed the computer program *gtdcom*, which extends the Geometrical Theory of Diffraction (GTD) propagation model to include realistic, three-dimensional terrain, broadband sounds (blast waves), and frequency weighting factors. This report describes the theoretical basis used to broaden the GTD model, and briefly outlines the use of *gtdcom*.

The new program was interfaced with the Geographic Resources Analysis Support System (GRASS) to calculate sound exposure levels (SELs) from blast sources using map elevation contour data. A user specifies the source position of the blast, a charge size, and an expected frequency weighting factor; the program calculates the SEL for each terrain cell, displays the results on the screen, and prepares a contour map for printer output.

The contents of this report are not to be used for advertising, publication, or promotional purposes. Citation of trade names does not constitute an official endorsement or approval of the use of such commercial products. The findings of this report are not to be construed as an official Department of the Army position, unless so designated by other authorized documents.

DESTROY THIS REPORT WHEN IT IS NO LONGER NEEDED

DO NOT RETURN IT TO THE ORIGINATOR

USER EVALUATION OF REPORT

REFERENCE: USACERL Technical Report EC-93/02, *Sound Exposure Level Prediction for Impulse Sound Sources Above Variable Terrain*

Please take a few minutes to answer the questions below, tear out this sheet, and return it to USACERL. As user of this report, your customer comments will provide USACERL with information essential for improving future reports.

1. Does this report satisfy a need? (Comment on purpose, related project, or other area of interest for which report will be used.)

_____

_____

_____

2. How, specifically, is the report being used? (Information source, design data or procedure, management procedure, source of ideas, etc.)

_____

_____

3. Has the information in this report led to any quantitative savings as far as manhours/contract dollars saved, operating costs avoided, efficiencies achieved, etc.? If so, please elaborate.

_____

_____

4. What is your evaluation of this report in the following areas?

   a. Presentation:_____

   b. Completeness:_____

   c. Easy to Understand:_____

   d. Easy to Implement:_____

   e. Adequate Reference Material:_____

   f. Relates to Area of Interest:_____

   g. Did the report meet your expectations?_____

   h. Does the report raise unanswered questions?_____

i. General Comments. (Indicate what you think should be changed to make this report and future reports of this type more responsive to your needs, more usable, improve readability, etc.)

_____

_____

_____

_____

_____

5. If you would like to be contacted by the personnel who prepared this report to raise specific questions or discuss the topic, please fill in the following information.

Name: _____

Telephone Number: _____

Organization Address: _____

_____

_____

6. Please mail the completed form to:

Department of the Army
CONSTRUCTION ENGINEERING RESEARCH LABORATORIES
ATTN: CECER-IMT
P.O. Box 9005
Champaign, IL 61826-9005

REPORT DOCUMENTATION PAGE

Form Approved
OMB No. 0704-0188

1. AGENCY USE ONLY (Leave Blank)	2. REPORT DATE	3. REPORT TYPE AND DATES COVERED
	May 1993	Final

4. TITLE AND SUBTITLE
Sound Exposure Level Prediction for Impulse Sound Sources Above Variable Terrain

5. FUNDING NUMBERS
PE 4A162720
PR A896
WU NN-TP0

6. AUTHOR(S)
Hong C. Zhuang, Leslie J. Benson, and Michael J. White

7. PERFORMING ORGANIZATION NAME(S) AND ADDRESS(ES)
U.S. Army Construction Engineering Research Laboratories (USACERL)
P.O. Box 9005
Champaign, IL 61826-9005

8. PERFORMING ORGANIZATION REPORT NUMBER
TR-EC-93/02

9. SPONSORING/MONITORING AGENCY NAME(S) AND ADDRESS(ES)
Office of the Chief of Engineers (OCE)
ATTN: ENVR-E
20 Massachusetts Avenue, NW
Washington, DC 20001

10. SPONSORING/MONITORING AGENCY REPORT NUMBER

11. SUPPLEMENTARY NOTES

Copies are available from the National Technical Information Service, 5285 Port Royal Road, Springfield, VA 22161

12a. DISTRIBUTION/AVAILABILITY STATEMENT
Approved for public release; distribution is unlimited.

12b. DISTRIBUTION CODE

13. ABSTRACT (Maximum 200 words)

The influence of the ground surface makes it difficult to calculate the propagation of impulse noise from Army-type blasts such as that produced by heavy-weapons fire on training ranges. This study developed the computer program *gtdcom*, which extends the Geometrical Theory of Diffraction (GTD) propagation model to include realistic, three-dimensional terrain, broadband sounds (blast waves), and frequency weighting factors. This report describes the theoretical basis used to broaden the GTD model, and briefly outlines the use of *gtdcom*.

The new program was interfaced with the Geographic Resources Analysis Support System (GRASS) to calculate sound exposure levels (SELs) from blast sources using map elevation contour data. A user specifies the source position of the blast, a charge size, and an expected frequency weighting factor; the program calculates the SEL for each terrain cell, displays the results on the screen, and prepares a contour map for printer output.

14. SUBJECT TERMS
gtdcom
blast noise
geometrical theory of diffraction propogation model

15. NUMBER OF PAGES
54

16. PRICE CODE

17. SECURITY CLASSIFICATION OF REPORT	18. SECURITY CLASSIFICATION OF THIS PAGE	19. SECURITY CLASSIFICATION OF ABSTRACT	20. LIMITATION OF ABSTRACT
Unclassified	Unclassified	Unclassified	SAR

FOREWORD

This study was performed for the Office of the Chief of Engineers (OCE) under Project 4A162720A896, "Base Facility Environmental Quality"; Task NN; Work Unit TP0, "Open Structure Propagation and Range Siting." The OCE technical monitor was LTC Hans Graven, ENVR-E.

This research was performed by the Acoustics Team (EAC), Environmental Compliance Modeling and Simulation Division, Environmental Sustainment Laboratory (EL). U.S. Army Construction Engineering Research Laboratories (USACERL). The USACERL principal investigator was Leslie Benson. USACERL assistant investigators were Dr. Hong Zhuang and Dr. Michael White. Assistance was also provided by Dr. George Swenson, Dr. Wang C. Chew, Dr. Bijan Houshmand, and Dr. Qing H. Liu, of the University of Illinois at Urbana-Champaign. Special appreciation is owed to the following USACERL personnel for providing help with the GRASS (Geographic Resources Analysis Support System) tools used in this study: James Westervelt, Michael Shapiro, Mary Martin, David Gerdes, Mark Johnson, and Russ Hougland. Dr. Paul D. Schomer is team leader, CECER-EAC. Dr. Diane K. Mann is Acting Chief, CECER-EC, and Dr. William Goran is Acting Chief, CECER-EL. The USACERL technical editor was William J. Wolfe, Information Management Office.

COL Daniel Waldo, Jr., is Commander and Director of USACERL, and Dr. L.R. Shaffer is Technical Director.

CONTENTS

FIGURES

FIGURES (Cont'd)

TABLES

TABLES (Cont'd)

SOUND EXPOSURE LEVEL PREDICTION FOR IMPULSE SOUND SOURCES ABOVE VARIABLE TERRAIN

1 INTRODUCTION

Background

Blast noises from the use of heavy weapons on Army training ranges may propagate over several kilometers, adversely affecting surrounding communities. Being able to calculate the effects of Army-type blasting would help Army planners to locate ranges or schedule training where and when it would cause the least disturbance. However, the influence of ground surface makes it difficult to calculate the sound wave propagation or the prediction of sound exposure level (SEL) of a point-acoustic source. Even if a rigid ground surface is assumed, the reflection and diffraction of sound waves by realistic terrain still makes the calculation very complicated. It is similarly difficult to calculate electromagnetic-wave propagation near the ground surface. Luebbers (1985) overcame this difficulty by using a propagation model based on Geometrical Theory, or ray theory, of Diffraction (GTD) for electromagnetic waves. Although acoustic waves usually have much lower frequencies than elecromagnetic waves, the ray theory of sound waves has been an efficient and realistic model for the propagation of acoustic waves. Later research extended the model to include acoustic wave propagation over hills and ridges (Houshmand 1990). Although the acoustic-wave GTD model represents a significant step towards more accurate numerical calculations, several important features must be added to the model before it can be applied to realistic situations.

The GTD program uses a two-dimensional model. The terrain is modeled as a piecewise, linear, two-dimensional structure of rectangular plates. (Although the terrain is only two-dimensional, the source and receiver can be located anywhere above the surface.) In modeling realistic terrain, the surface can be specified as an arbitrary assembly of plates, each having any aspect and slope.

Objectives

The objectives of this work were to extend the GTD propagation model to include realistic terrain, to use the improved model to map the spatial SEL prediction of a given explosive source above a specified terrain, and compare those predictions to measured data.

Approach

A literature search was conducted to locate an appropriate mathematical strategy for modeling sound-wave propagation over realistic terrain. The (GTD) model of Luebbers was adapted to include realistic terrain, broadband sounds (blast waves), and frequency weighting factors. The improved model was interfaced with the Geographic Resources Analysis Support System (GRASS) to calculate the SEL from impulse sources, given the map elevation contours.

Mode of Technology Transfer

The results of this study will be used as baseline guidance in future work in predicting propagation over rough or variable terrain.

2 THE RAY THEORY

Since the discovery of Newton's three laws of motion in 1687, people have been accustomed to consider motion as something that occurs along a certain path. The propagation of waves in an extended medium has been considered as motion of perturbation along a path of rays; this is known as ray theory. Under the ray theory, concepts such as refraction, reflection, and diffraction are easily understood. The path of rays can be mechanically traced by Snell's law.

In geometrical theory, the rays along which the waves propagate in a homogeneous medium are rectilinear and, upon striking the boundary between two such media, are reflected back into the original medium or refracted into another medium according to certain simple rules. The rules are valid in the approximation only if path differences of the order of a wavelength can be neglected.

From the standpoint of wave theory, the concept of a wavefront plays a central role in the geometrical theory or ray theory. A wavefront is any moving surface along which a waveform feature is being simultaneously received. It is not necessarily assumed that the amplitude along a wavefront is constant, or that the wavefront is planar. However, geometrical theory assumes that the amplitude varies only slightly over distances comparable to a wavelength and that the radii of curvature of the wavefront are substantially larger than a wavelength.

Although audible sound waves have much larger wavelengths (17 cm to 17 m) than, for example, the wavelength of visible light, which occupies a range in the neighborhood of 50 μm, there is still wide use of geometrical acoustics or ray acoustics, which developed as an important branch of acoustical theory (Pierce, 1989). Ray acoustics is an approximation in the same sense as is geometrical optics, in that, within the range of a wavelength, both the medium and the boundary are homogeneous. The influences of the actual spatial fluctuations of the medium or of the boundary are counted as noise or perturbation on the results.

Luebbers (1985) developed a computer model, the "GTD propagation model," to compute the electric field from a dipole antenna, the source point, radiating above a piecewise linear two-dimensional terrain structure where each linear segment of the structure may have arbitrary permittivity, conductivity and surface roughness. The model computes the total complex electric field at the field point (the observation point) by locating and summing all of the rays of the electromagnetic waves that can propagate from the source dipole to the field point either directly or by interaction with the linearized terrain profile. The individual rays contributing to the electric field may be obtained separately, so that the user can obtain information as to how most of the energy is reaching the field point, for example, by reflection from a certain area or diffraction over a particular ridge.

The Luebbers's ray propagation model was intended for use in the frequency range of 100 MHz to 10 GHz. Houshmand, et al. (1990) extended the GTD propagation model to acoustic wave propagation. A vector electric field calculated is replaced by a scalar sound pressure. However, Houshmand's model accounts only for a restricted model for the terrain, such that the terrain is composed of an assembly of parallel ridges or valleys. This structure can be specified as height as a function of one coordinatre only: that running perpendicular to the ridges. This report relaxes the assumption to a more realistic model. In this new model, the terrain can be specified as an arbitrary function of position limited only by the grid size. The SEL computation may still be accomplished with the theory of ray acoustics. Any inhomogeneity of the terrain within the order of the grid size is considered as "roughness" of the terrain surface. Although ray acoustics may be not as good in this case as wave theory because of the low frequency of sound waves, the geometrical method should not be ignored as a way to estimate SEL.

Two-Dimensional GTD Propagation Model

Figure 1 shows an example of a parallel terrain profile that has already been linearized for conducting a ray calculation (Luebbers, 1985). In this example, 15 points make up a profile consisting of 14 connecting segments. Remember that in any direction x, perpendicular to the paper, the terrain is infinite. Each point represents an edge, and each segment represents a plate of terrain surface. After inputting the terrain parameters, the location of the wave source, and observation points, and the frequency, the model traces all the rays that can exist and judges those rays that can propagate from the source point to the observation point. The complex amplitudes of all the rays that can be received at the observation point are summed up to obtain the final wave amplitude and phase. Several of the types of rays included in the model are illustrated in Figures 2 to 5. These figures show that the direct ray of Figure 2 propagates directly from the source to the observation point, the reflected ray of Figure 3 is reflected once from the terrain, and that the reflected-diffracted ray of Figure 4 is reflected once and subsequently diffracted once on its path to the observation point. In Figure 5, we see a reflected-diffracted-reflected ray that reflected from Plate K to Edge e, then diffracted from Edge e to Plate M, and finally reflected from Plate M to the observation point, a human listener, for example. The GTD model considers 16 types of rays (Table 1).

The theoretical basis for determining direction of reflection of rays is simply to make the angle of incidence equal to the angle of reflection. The amplitude and phase of the reflected electromagnetic waves is determined by the complex-valued reflection coefficient, computed using the angle of incidence, electrical constants of the reflecting segment, and a roughness factor representing height variability in local

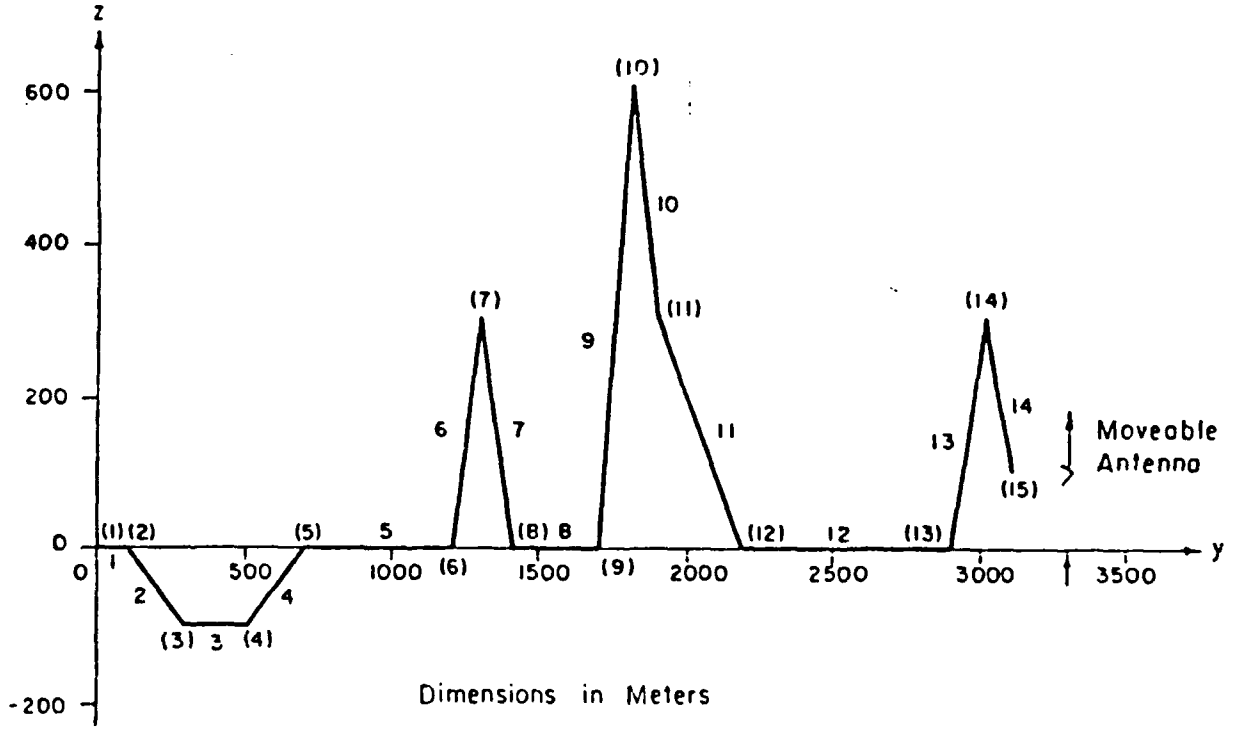

Figure 1. Sample Terrain Profile That Allows All 16 Types of Rays Included in Table 1 of the GTD Model.

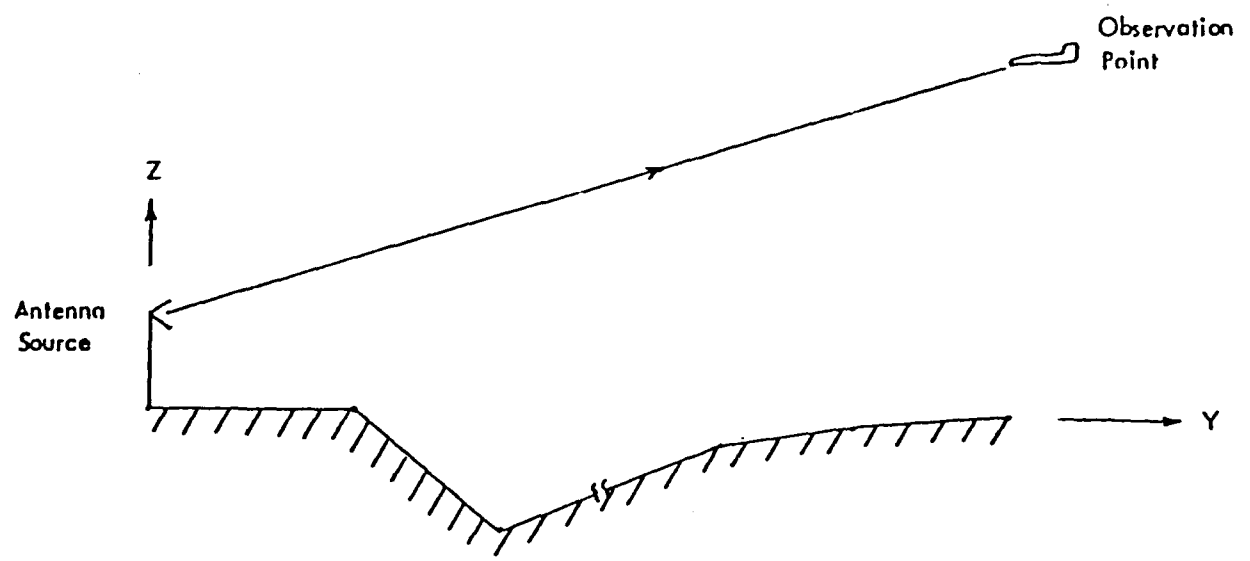

Figure 2. **The Direct Ray That Propagates Directly From the Source Point to the Observation Point.**

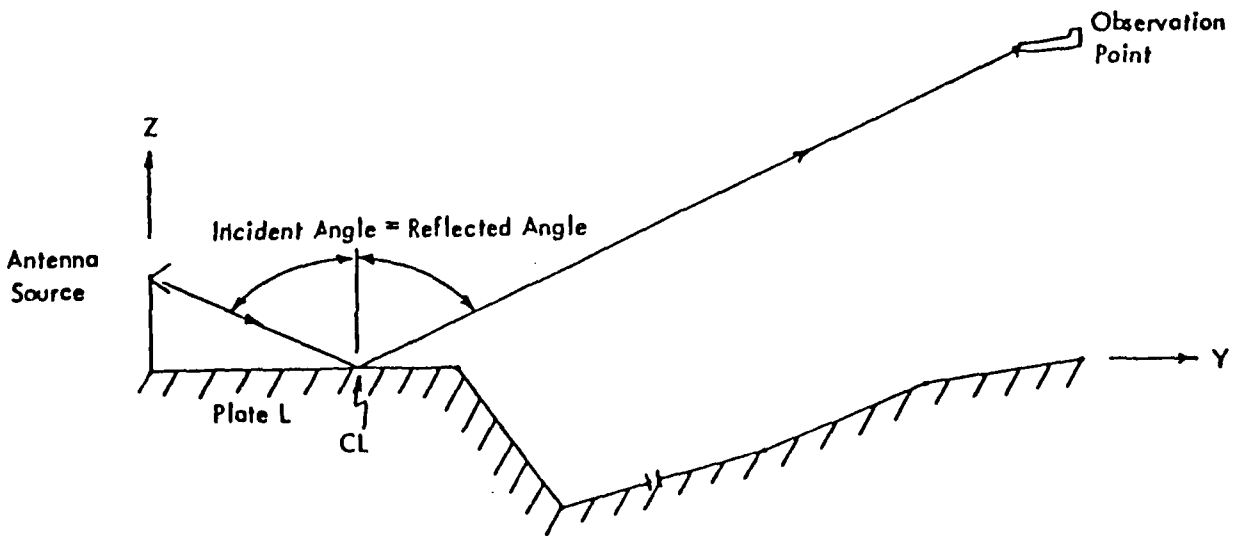

Figure 3. The Singly-Reflected Ray Reflected From Plate L to the Observation Point.

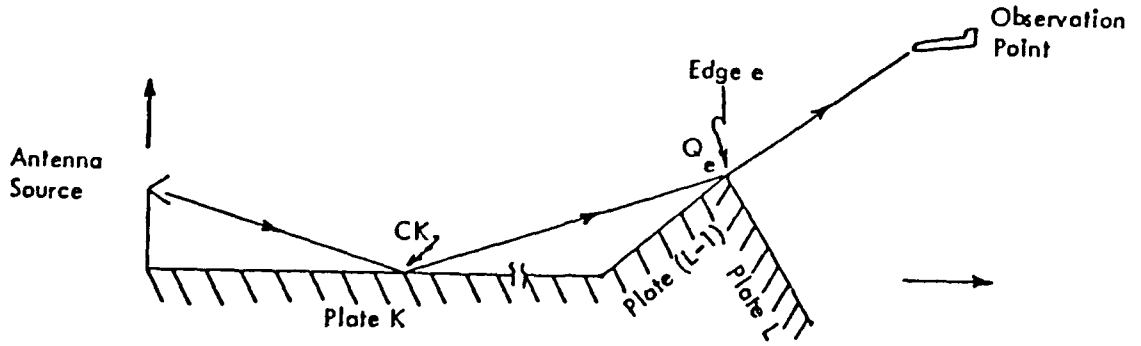

Figure 4. **The Reflected-Diffracted Ray Reflected From Plate K to Edge e, and Diffracted From Edge e to the Observation Point.**

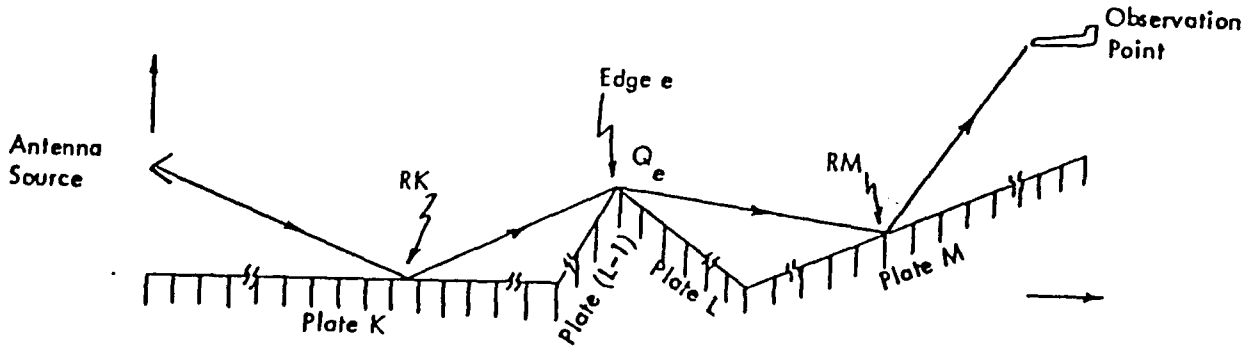

Figure 5. **The Reflected-Diffracted-Reflected Ray Reflected From Plate K to Edge e, Diffracted From Edge e to Plate M, and Reflected From Plate M to the Observation Point.**

Table 1

Types of Rays Included in the GTD Model

```
JDIR-----Direct ray;
JREF-----Reflected rays;
JRR------Reflect twice;
JRD------Reflect, then diffract;
JRRD-----Reflect twice, then diffract;
JRDR-----Reflect, diffract, then reflect;
JDIF-----Diffract once;
JDR------Diffract, then reflect;
JDRD-----Diffract, reflect, then diffract;
JDD------Diffract twice;
JDDR-----Diffract twice, then reflect;
JDRR-----Diffract, then reflect twice;
JRDD-----Reflect, then diffract twice;
JRRR-----Reflect three times;
JDDD-----Diffract three times;
JRDDD----Reflect, then diffract three times.
```

terrain, such as variability caused by vegetation, uneven ground, or waves (if propagation is over water). The roughness factor is used to modify the reflection coefficient to account for imperfect reflection caused by local terrain roughness. Specifically, the modified reflection coefficient for a rough surface used by the GTD model is defined as the plane-wave reflection coefficient for specular reflection from a flat smooth surface multiplied by a surface roughness factor δ. The surface roughness factor can be found from the standard deviation ΔG of the terrain elevation along each piecewise-linear section of terrain defining the profile as follows:

$$\delta^2 = e^{-\Delta\Phi^2} \qquad \text{[Eq 1]}$$

with

$$\Delta\Phi = \frac{4\pi\Delta G}{\lambda}\sin\gamma \qquad \text{[Eq 2]}$$

where γ is the grazing angle and λ is the wavelength. In Eqs 1 and 2, $\Delta\Phi$ represents the phase shift between the shortest and longest reflected path from an ensemble of rays that strike the rough surface.

For diffraction, the basic approach taken is to approximate each change in slope in the piecewise-linear approximation to the terrain profile as a wedge. Wedge diffraction solutions have been available since the beginning of the century, but have not been widely used for propagation path loss predictions due to their complexity. A numerically simple and elegant solution to wedge diffraction which serves as a canonical problem in the geometrical theory of diffraction was published by Keller (1962) 30 years ago. However, it was not suitable for general application to radio propagation over diffracting edges, since it fails in the vicinity of shadow boundaries, i.e., when the source, edge and field point lie near a straight

line. This shortcoming was eliminated by Kouyoumjian and Pathak (1974) in their formulation of a wedge diffraction coefficient, which is valid at shadow and reflection boundaries.

As originally formulated, the diffraction coefficients were limited to perfectly conducting wedges. A heuristic extension that allows the approximate treatment of finitely conducting locally-rough wedge diffraction has been made by Rojas-Teran and Burnside (1981), Chamberlin and Luebbers (1982) and Luebbers, et al. (1982). Luebbers (1985) further made modifications to the usual wedge diffraction coefficients nessessary to include finite conductivity and local surface roughness. The amount of diffracted energy re-radiated from an edge is determined by the diffraction coefficient, which is a function of the wedge angle and the incident and diffracted ray geometries. Note that all these considerations and modifications fit both electromagnetic waves and acoustic waves.

Ray Selection Algorithms for Two-Dimensional Situations

A computer is needed not only to be able to evaluate individual ray amplitudes, but also to check for blockage and to search for all possible combinations of each type of ray interactions with a given terrain profile and then to combine them to get the total field at the observation point.

Direct Ray

The direct ray is the most significant, if it exists, and is defined as the ray that travels directly from the original source to the observation point. This ray can exist only if there is no terrain high enough to block its path of travel. Since the actual terrain is approximated by many finite flat plates, the computer program must logically test the ray for blockage by any of these plates. If the ray is not blocked, then its associated wave field is calculated, and it becomes the first wave field contribution included in the total wave observed.

Singly-Reflected Ray

A singly-reflected (R) ray is defined as a ray reflected once from a plate, where the incident angle of the ray with respect to the plate is equal to the reflected angle. To test for the existence of the ray, the first step is to find the image source location. This image source is uniquely determined by the original source and the unit normal to the plate. After the image source is found, the ray is assumed to radiate from this source to the observation point, with its amplitude multiplied by the appropriate reflection coefficient. The second step is to determine whether or not the ray has an interception point within the physical boundaries of the plate. Also, the ray must not be blocked by the other plates. Once this ray passes all of the tests, its wave field is calculated and vectorially added to previous contributions. This computer algorithm is again performed on the next plate until all of the plates have been included. The final result is the total singly-reflected wave field.

Singly-Diffracted Ray

Diffraction is the phenomenon that occurs when the wave ray is incident on any discontinuity in the geometry of an object, i.e., a sharp corner or an edge. One of the important stages in the process of finding the diffracted wave field is to locate the diffraction point, Q_e (Figure 6). Q_e is the point where the angle between the line from the source to Q_e and the diffracting edge is equal to the angle between the diffracting edge and the line from Q_e to the observation point. In other words, Q_e is the point that satisfies the Law of Edge Diffraction (Fermat's Principle).

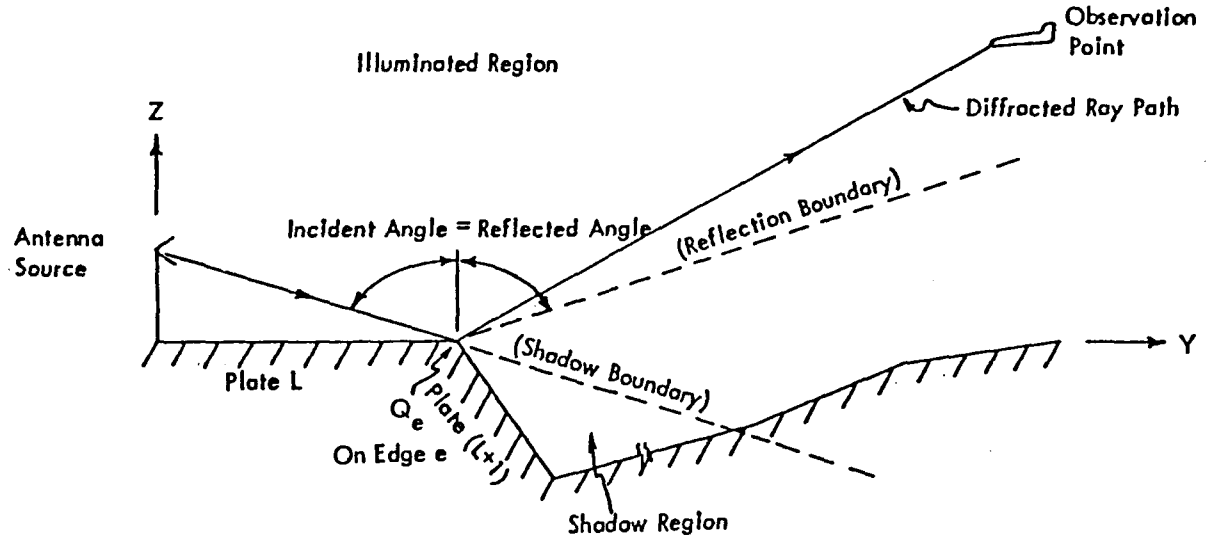

Figure 6. The Singly-Diffracted Ray Diffracted From Edge e to the Observation Point.

Once Q_e is found, the logical test for ray existence is performed. Let Plate L and Plate L+1 form a wedge e, as shown in Figure 6. Edge e is tested for the existence of a diffraction point. The computer program separates the terrain into two regions. The first region includes the first plate to plate L-1; the second region is from plate L+2 to the last plate. In the first region, the computer program tests for blockage using the source location and Q_e as the two end points of a ray. In the second region, Q_e and the obsevation point are the two end points, and similar blockage tests are performed. If the ray satisfies these blockage tests, the diffracted ray is evaluated, and the complex amplitude is added to the total. If the ray was blocked, the ray is abandoned. The program repeats the procedure until all of the edges have been tested for possible diffracted rays. The final result is the total singly diffracted field.

Doubly-Reflected Ray

The doubly-reflected (RR) ray is one that is reflected from two different plates. An example of this ray is shown in Figure 7, where the ray is reflected from Plate L to Plate M, and reflected off Plate M to the observation point. The existence determination algorithm starts with the location of the doubly-imaged source. First, the image of the original source is found with respect to Plate L, treat this image source as though it were the actual source, and find its reflection with respect to Plate M. The RR ray radiates from this doubly-imaged source to the observation point, but with its amplitude multiplied by the two reflection coefficients. A line from the doubly-imaged source through the observations point intersects Plate M at the reflection point (CM). If CM is located outside the physical boundaries of Plate M, the RR ray does not exist. But if CM lies within the boundaries, the reflection point on Plate L (CL) must be found. The first imaged source and CM form a ray, whose reflection point CL must lie on the Plate L. If CL and CM exist, the blockage tests are performed. In summary, for the RR ray to exist, interception points CL and CM must lie on both plates, and the lines of sight from the original source to CL, from CL to CM, and from CM to the observation point must not be blocked. If these conditions are met, the RR ray wave amplitude and phase are calculated and added to the previous contributions. This process

is repeated until all of the possible plate combinations have been tested. The final result is the total doubly-reflected field.

Reflected-Diffracted Ray

The reflected-diffracted (RD) ray is the ray that is reflected once from a Plate K and then diffracted once by an Edge e. An example of such a ray is shown in Figure 8.

The existence of a reflection point (CK) and the diffraction point (Q_e) is the first requirement for an RD ray to exist. There are at least two possible methods to determine the existence of these two points. The first method involves creating images of the edge under test and the observation point with respect to an extension of the reflecting plane being tested (K in this case). The geometries involved in the first method are shown in Figure 9a. With the source location, image edge, and image observation point, the location of the diffraction point on the (image) edge is calculated. Finally, if a line between the source and the image of Q_e intersects the Plane K, CK exists, and the ray is tested for blockage.

The second method (see Figure 9b) is to image the source rather than the diffraction point. For this method, a line between the source image and Q_e intersecting Plane K determines the existence of Q_e and CK. Due to computational considerations, the latter method is considered desirable and is used in the model, although both methods give identical results.

If CK and Q_e exist, the blockage algorithm is performed. If the ray is not blocked, RD ray wave amplitude and phase are calculated and added to the previous contributions. The amplitude is also multiplied by the appropriate reflection coefficient.

This process is repeated until all plate and edge combinations for the RD ray have been tested. The final result is the total reflected-diffracted field.

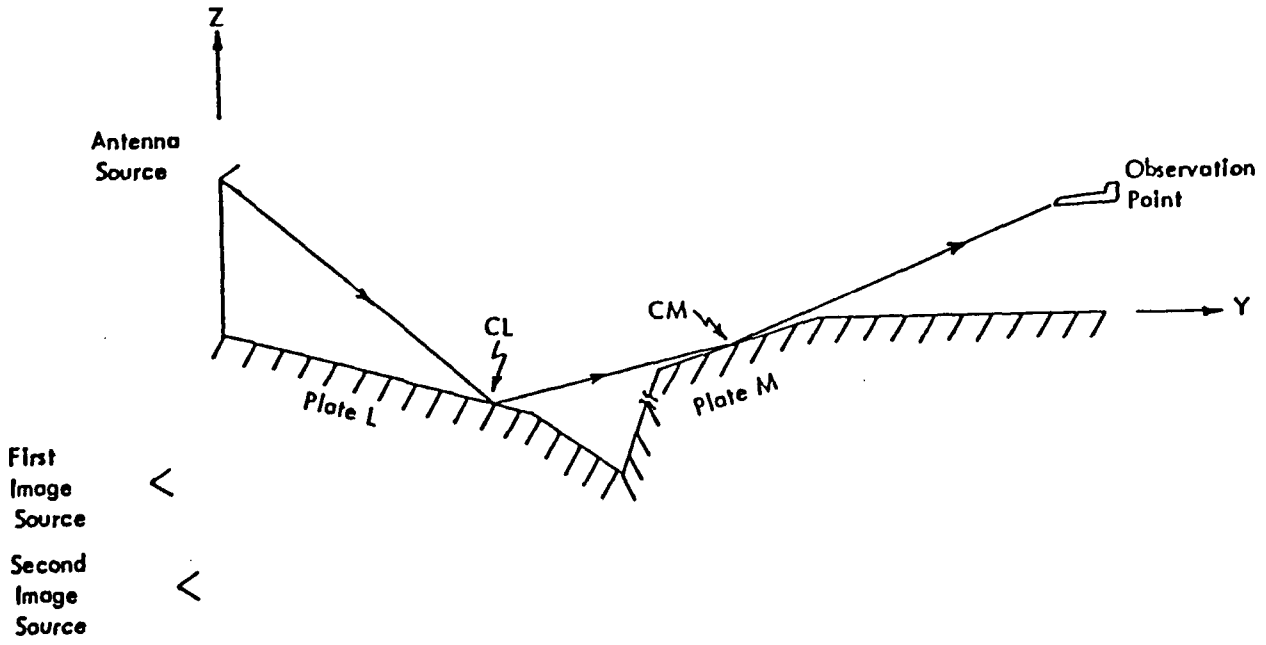

Figure 7. The Doubly-Reflected Ray Reflected From Plate M, and Reflected From Plate M to the Observation Point.

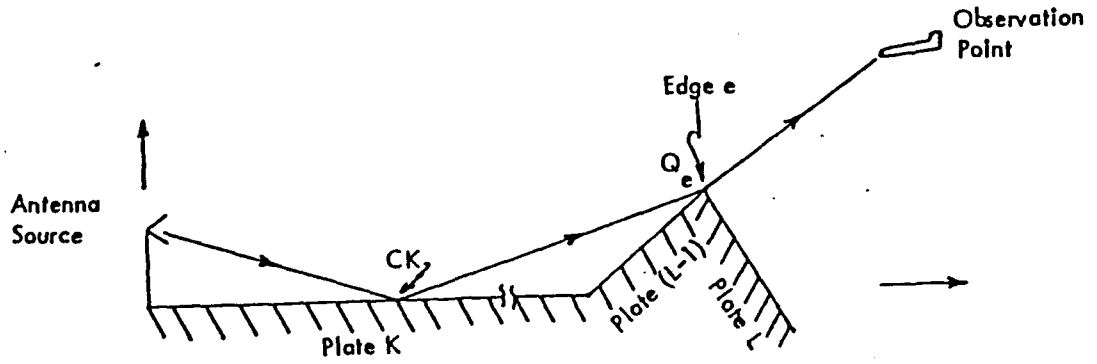

Figure 8. **The Reflected-Diffracted Ray Reflected From Plate K to Edge e, and Diffracted From Edge e to the Observation Point.**

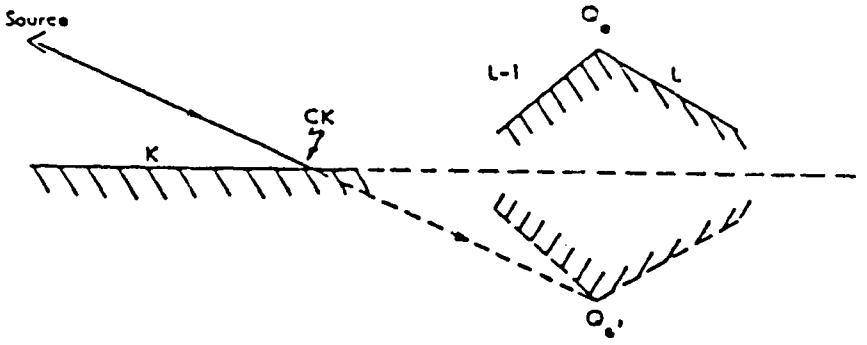

(a)

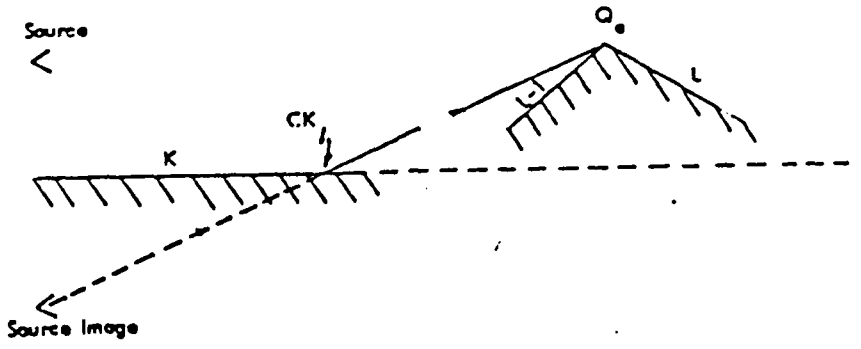

(b)

Figure 9. **Two Methods for Determining the Existence of a Diffraction Point (Qe) for a Possible Reflected-Diffracted Ray Reflected From Plate K and Diffracted at Edge e.**

Diffracted-Reflected Ray

The diffracted-reflected (DR) ray is diffracted from an edge and reflected (off a plate), which is not one of the two plates that make up the edge. The ray geometry is illustrated in Figure 10. The first requirement for a DR ray to exist is that the diffraction point and reflection point must exist. There are two possible methods to determine the existences of these two points.

The first method involves reflecting the source and the edge (e in this case) with respect to an extension of the plate under test (L in this case). Figure 11a depicts the geometry involved in this method. The image of the diffraction point is determined from an image source location, an image Edge e and the observation point. Using the diffraction point image and the observation point as two end points, together with a plane that contains Plate L, reflection point (CL) is calculated. Finally, Q_e is determined by reflecting the image of the diffraction point with respect to Plate L.

The second method is to reflect the observation point with respect to the plane containing Plate L (see Figure 11b). With the source location, the edge, and the image of the observation point, Q_e is determined using the same logic as for the singly-diffracted ray. CL is found by using Q_e and the image of the observation point as two end points of a line that intercepts an extension of Plate L.

A comparison of these two methods indicated that the latter method required fewer computational steps, hence less computation time. Therefore, the latter method is used.

After Q_e and CL are determined to exist, the second requirement is that the line of sight from the source location to Q_e from Q_e to CL, and from CL to the observation point must not be blocked. If the line of sight is not blocked, the DR ray wave amplitude and phase are calculated and added to the previous contributions. The DR ray is also multiplied by the reflection coefficient for Plate L. This process is repeated until all edge and plate combinations for the DR ray have been tested. The final result is the total diffracted-reflected field.

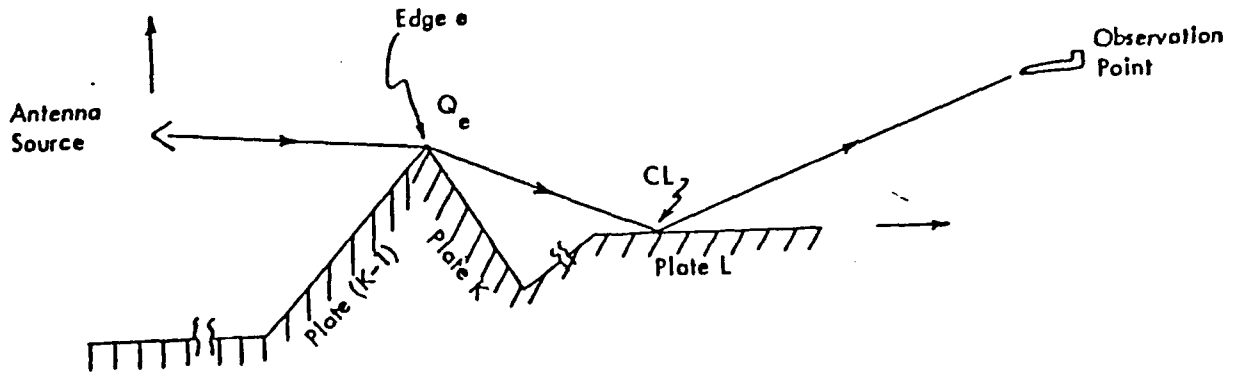

Figure 10. The Diffracted-Reflected Ray Diffracted From Edge e to Plate L and Reflected From Plate L to the Observation Point.

Doubly-Diffracted Ray

The doubly-diffracted (DD) ray is diffracted by two different edges. An example of this ray is shown in Figure 12, where the first edge is formed by connected Plates K and K-1, and the second edge is formed by Plate L and Plate L-1.

Before starting the blockage test, the two diffraction points DK and DL have to be determined. If both DK and DL exist, testing for blockage of the line of sight from the source to DK, DK to DL, and DL to the observation point is performed. If there is not line of sight blockage, the DD ray exists, and its associated wave field components are calculated. This process is repeated until all of the edges have been tested. The final result is the total doubly-diffracted field.

Triply-Reflected Ray

The triply-reflected (RRR) ray is defined as any ray reflected from plates three times, with the incident and reflected angles on each plate equal. Figure 13 shows an example of such a ray.

To test for the existence of the ray, the first step is to find the image-source location sound source with respect to the first reflecting plate (K in this case). The method of determining the image source location is the same as for previous rays involving reflection. Once the image location is found, using it as a source, a second image with respect to Plate L is located. Then using the second image as if it were the source, a third image point with respect to Plate M is located.

The second step is to determine whether or not reflection points exist within the physical boundaries of Plate K, L, and M. This can be ascertained by using the third image and the observation points as two points on a line. This line must intercept Plate M; the interception point (RM) and the second image location are then used as two points on a line that must intercept Plate L. Again, by using the interception point on Plate L (RL) and the first image location as two end points on a line, the third interception point (RK) is found and must be located on Plate K. If any one of the three reflection points, RK, RL, and RM is not located within the appropriate plate boundary, the RRR ray does not exist and the next reflecting plate M+1 is considered.

If three reflection points exist, the third step is to determine whether or not the ray that travels from the source to RK, from RK to RL, from RL to RM, and from RM to the observation point is blocked by the other plates.

If the RRR ray passes all blockage tests, its wave amplitude and phase are calculated and added to the previous contributions. This algorithm is performed on all combinations of plates. The final result is the total triply-reflected field.

Reflected-Reflected-Diffracted Ray

The reflected-reflected-diffracted (RRD) ray is defined as a ray reflected by two different plates, then diffracted from an edge, which must not be part of the two reflecting plates, to the observation point. An example of this ray is given in Figure 14.

The first step to test for the existence of the ray is to find the image source position with respect to Plate K. Once the first image point is found, the second image point must be calculated using the first image location and Plate L. Using the second image location and an edge (Edge e in this case) the diffraction point is determined.

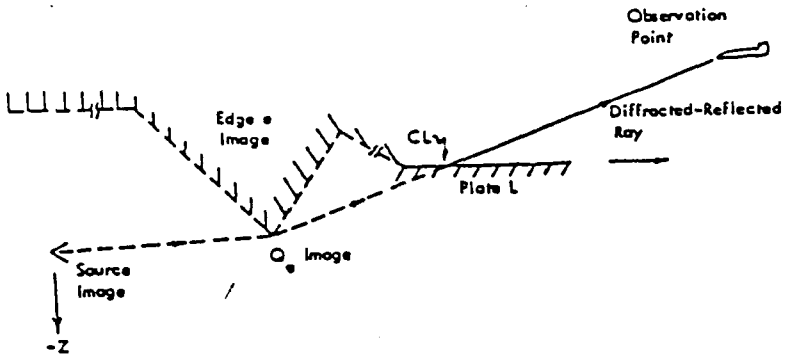

(a)

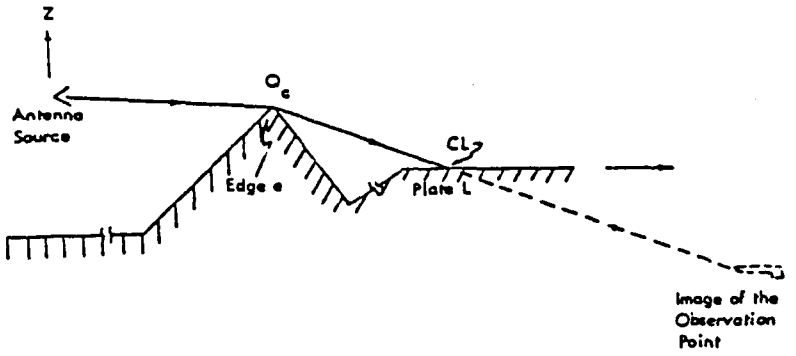

(b)

Figure 11. Two Methods for Determining the Diffracted-Reflected Ray Path.

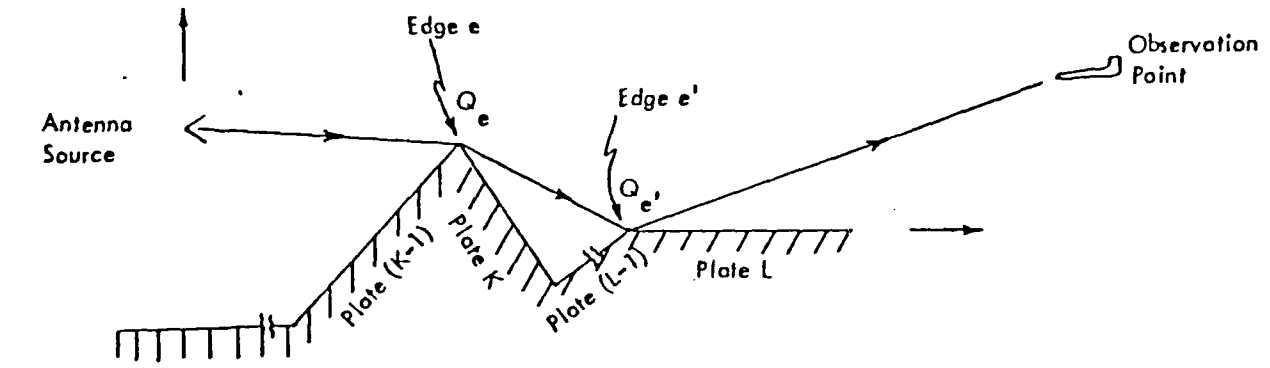

Figure 12. **The Doubly-Diffracted Ray Diffracted From Edge e to Edge e′, and Diffracted From Edge e′ to the Observation Point.**

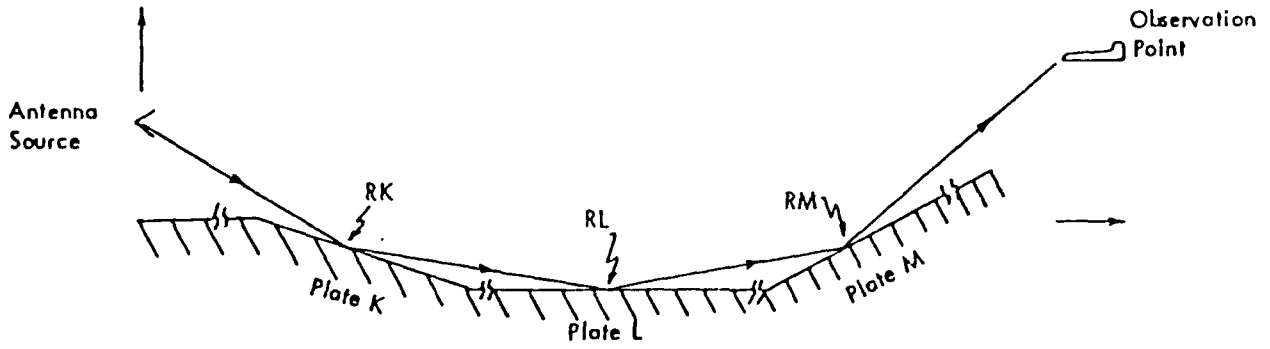

Figure 13. **The Triply-Reflected Ray Reflected From Plate K to Plate L, Reflected From Plate L to Plate M, and Reflected From Plate M to the Observation Point.**

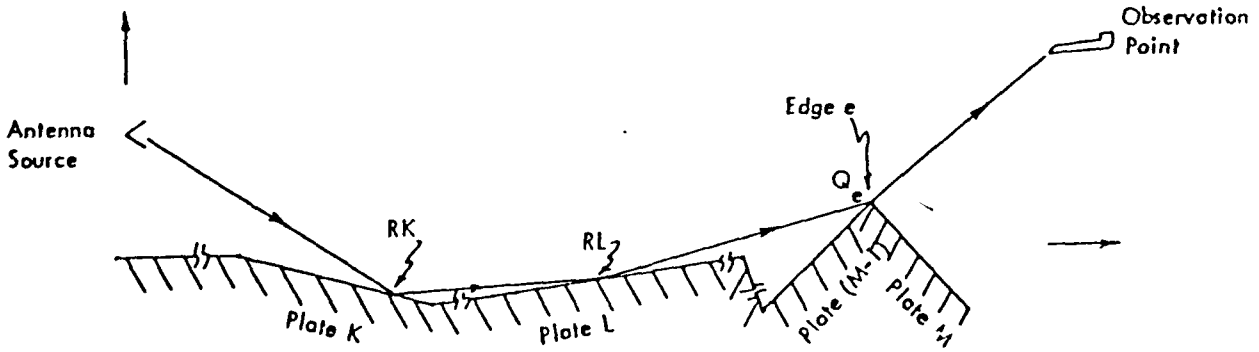

Figure 14. **The Reflected-Reflected-Diffracted Ray Reflected From Plate K to Plate L, Reflected From Plate L to Edge e, and Diffracted From Edge e to the Observation Point.**

The second step is to determine whether reflection points exist within Plates K and L, and a diffraction point (Q_e) on Edge e. With the exception of the case of an edge and a line that contains the second image point and the observation being parallel, the diffraction point always exists in the two-dimensional case. Q_e and the second image location are used as two points on a line. The reflection point (RL) where this line intercepts Plate L is found. Then using RL and the first image location as two points on a line, the reflecting point RK, which is the interception point on Plate K, is calculated. If either RL, RK, or Q_e do not exist, the RRD ray will not exist.

The third step is to test whether or not the ray from the source to RK, RK to RL, RL to Q_e, and Q_e to the observation point is blocked by the other plates. If an RRD ray passes the existence tests, its wave amplitude and phase are calculated and added to the previous contributions. This algorithm is performed on all forward-traveling ray combinations of plates and edges. The final result becomes the total reflected-reflected-diffracted wave field.

Reflected-Diffracted-Reflected Ray

The reflected-diffracted-reflected (RDR) ray is reflected once from a plate, diffracted by an edge that is not part of the plate, and reflected once more from another plate. Figure 15 depicts an RDR ray.

The first step in the ray existence tests is to determine that the edge (Edge e in this case) is located above both reflecting plates (Plates K and M are considered). If this condition is met, the source and observation point are imaged with respect to Plate K and Plate M, respectively; also, an image of Edge e with respect to Plate K is calculated. By using an image of Edge e, the image source and the image of the observation point, the image diffraction point (Q_ei) is determined. The method in determining the diffraction point is explained previously. Q_ei is then imaged again with respect to Plate K to a point on Edge e, and is the diffraction point (Q_e).

The second step is to test for the existence of the reflection points on Plates K and M. The reflection point on Plate K (RK) is determined by generating a line that contains Q_e and the image source, intercepting Plate K; similarly, the reflection point on Plate M (RM) is located where a line that contains Q_e and the image of the observation point intersects Plate M.

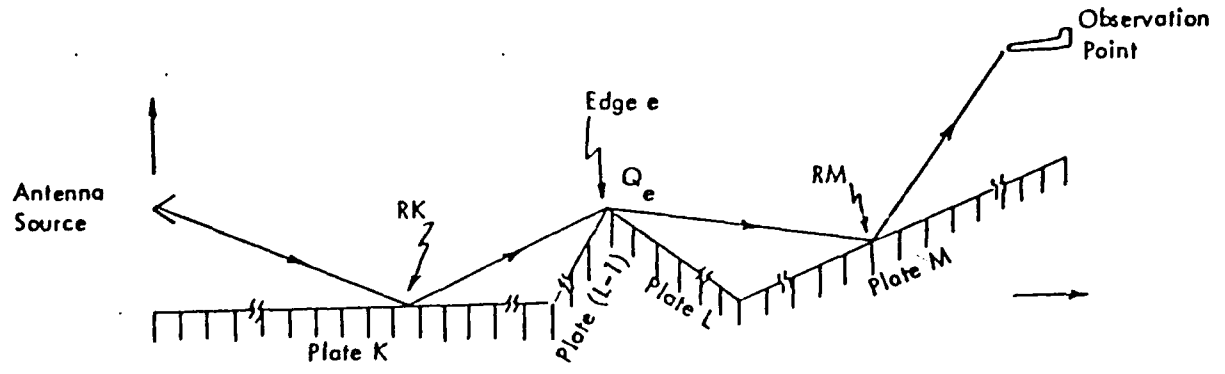

Figure 15. The Reflected-Diffracted-Reflected Ray From Plate K to Edge e, Diffracted From Edge e to Plate M, and Reflected From Plate M to the Observation Point.

Once RK and RM are determined to lie on Plates K and M, the last step required is the blockage test. The line of sight from the source to RK, from RK to Q_e, from Q_e to RM, and from RM to the observer must not be blocked by the other plates. If the ray passes the existence test, its wave amplitude and phase are calculated and added to the total. This process is repeated until all forward traveling ray combinations of plates and edges are examined. The final result becomes the total reflected-diffracted-reflected field.

Reflected-Diffracted-Diffracted Ray

The reflected-diffracted-diffracted (RDD) ray is defined as a ray reflected from a plate and diffracted from two different edges, where the diffraction edges are not part of the plate. An example of this ray geometry is given in Figure 16.

The first step to test for ray existence is to locate the image source with respect to Plate K. Once this image point is found, the diffraction points on Edges e and e′ are determined. The second step is to determine the existence of the reflection point (K in this case). This is done by generating a line that contains the image source and the diffaction point (e in this case) and testing whether it intercepts Plate K. The third step is the blockage test. A line that originates from the source to RK, from RK to Q_e, from Q_e to Q_e', and from Q_e' to the observation point must not be blocked by the other plates.

Once the ray passes the existence tests, its wave amplitude and phase are calculated and added to the previous contributions. This algorithm is performed on all forward-traveling ray combinations of existing plates and edges. The final result becomes the total reflected-diffracted-diffracted field.

Diffracted-Reflected-Reflected Ray

The diffracted-reflected-reflected (DRR) ray is diffracted once from an edge which must not be part of a reflecting plate, and reflected from two different plates. The ray geometry is illustrated in Figure 17.

The first step in the ray existence test is to determine that the diffraction point and both reflection points exist. This is done by reflecting the observer location with respect to Plate M, and further reflecting this image with respect to Plate L to form the secondary-image point. From the secondary-image observer

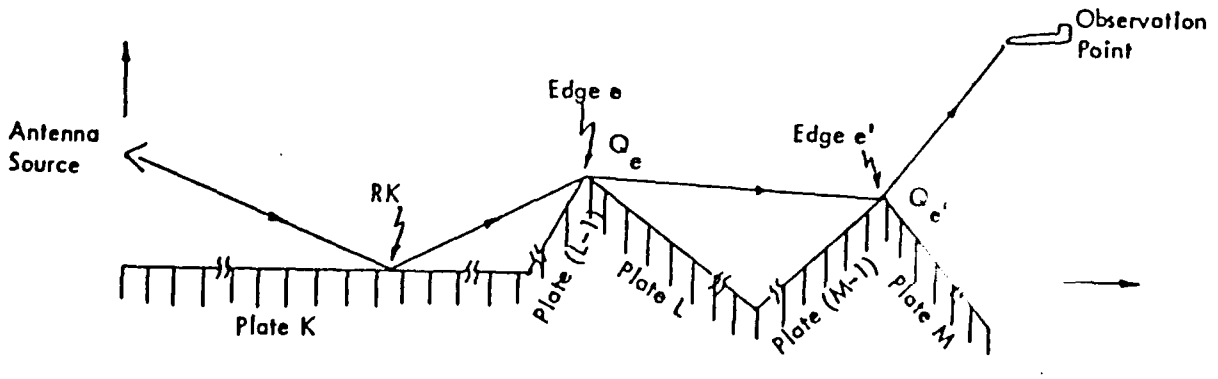

Figure 16. The Reflected-Diffracted-Diffracted Ray Reflected From Plate K to Edge e, Diffracted From Edge e to Edge e′, and Diffracted From Edge e′ to the Observation Point.

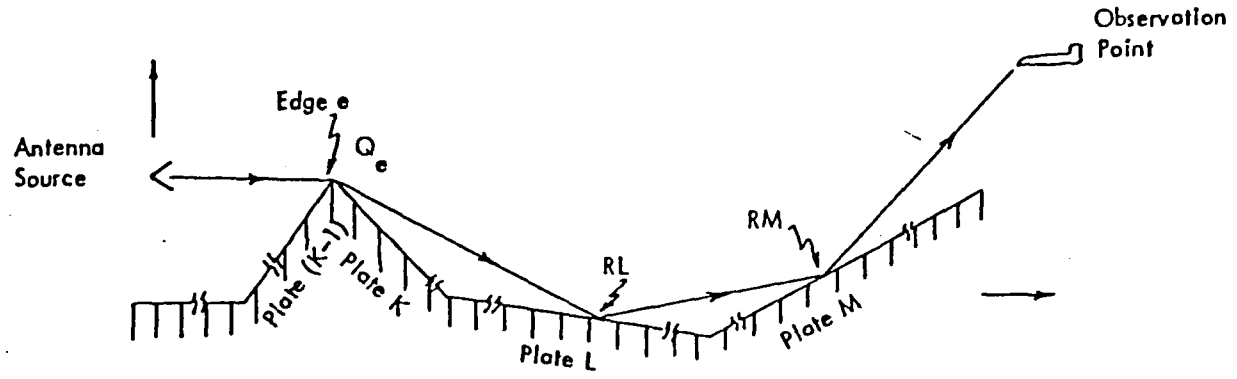

Figure 17. The Diffracted-Reflected-Reflected Ray Diffracted From Edge e to Plate L; Reflected From Plate L to Plate M, and Reflected From Plate M to the Observation Point.

point, the source, and the Edge e, the location of the diffraction point (Q_e) is calculated. The method of obtaining Q_e has been discussed previously. Q_e and the secondary-image observer location form a line, whose intersection point (RL) on the extension of Plate L is calculated; similarly, RL and the first image observation point form another line, whose intersection point (RM) on the extension of Plate M is determined. Both RL and RM must lie on Plates L and M for the DRR ray to exist.

The last step is the blockage test. Lines from the source to Q_e, from Q_e to RL, from RL to RM, and from RM to the observation point must not be blocked by the other plates. If the line is not blocked, the DRR ray wave amplitude and phase are calculated and added to the previous contributions.

The process is repeated until all edge and plates in forward-direction combinations for the DRR ray have been examined. The final result is the total diffracted-reflected-reflected field.

Diffracted-Reflected-Diffracted Ray

The diffracted-reflected-diffracted (DRD) ray is one that is diffracted from an edge, reflected from a plate that is not part of the same edge, and diffracted once more from another edge which is not part of the reflecting plate. An example of this ray geometry is illustrated in Figure 18.

The first condition to test the DRD ray is possible is that the diffraction points on both edges (e and e′ in this case) and the reflection point on a plate (L for example) must exist. One method is to reflect both Edge e′ and the observation point with respect to Plate L. Then, using the source, Edge e, image of Edge e′, and the image of the observation point, the diffraction points are determined as for the DD ray.

The second step is to test whether the reflection point is on Plate L. The reflection point is obtained by generating a line that contains both diffraction points and intersects Plate I at RL. For the DRD ray to exist, RL must be within the boundaries of Plate L. It should be noted that one diffraction point is on the image of Edge e′. Therefore, before starting blockage tests, the actual diffraction point is needed. The resultant point (Q_e') is thus located on Edge e′.

The final condition for the ray to exist is no blockage. The lines of sight from the source to Q_e, from Q_e to RL, from RL to Q_e', and from Q_e' to the observation point must not be blocked by other plates.

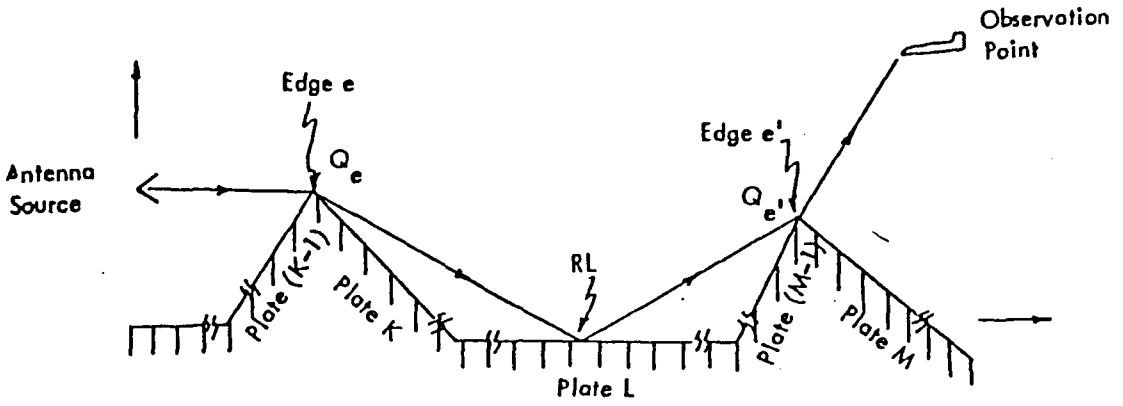

Figure 18. The Diffracted-Reflected-Diffracted-Ray Diffracted From Edges e, to Plate L, Reflected From Plate L to Edge e', and Diffracted From Edge e' to the Observation Point.

If not blocked, the ray wave amplitude and phase are calculated and added to the previous contributions. The process is repeated until all edges and plates in forward-direction combinations for the DRD ray have been tested. The final result is the total diffracted-reflected-diffracted field.

Diffracted-Diffracted-Reflected Ray

The diffracted-diffracted-reflected (DDR) ray is defined as a ray diffracted from two different edges and reflected once from a plate that does not touch those diffracting edges. An example of this ray geometry is illustrated in Figure 19.

The first step is to locate the image of the observation point with respect to the reflecting plate (Plate M in this case). The image location must lie below the plane that contains reflecting Plate M. If this condition is met, the next step is performed.

The second step is to find the image diffraction points on both edges (Edges e and e') and the reflection point. The method is very similar to the one used for the doubly-diffracted ray. The only difference is that instead of the real observation point, the image observation point is used. Once Q_e and Q_e' are found, the reflection point on Plate M is calculated. Q_e' and the image observation point form a line that intercepts the plane that contains Plate M. If the reflection point (RM) lies within Plate M, the blockage test is performed.

The blockage test is the last step in the ray existence algorithm. The lines of sight propagation path from the source to Q_e, from Q_e to Q_e', from Q_e' to RM, and from RM to the observation point must not be blocked by the other plates.

If the DDR ray passes all three steps, it exists and the wave amplitude and phase are calculated and added to the previous contributions. This algorithm is repeated on all forward-direction combinations of plates and edges. The final result becomes the total diffracted-diffracted-reflected field.

Triply-Diffracted Ray

The triply-diffracted (DDD) ray is diffracted by three different edges. An example of this ray is illustrated in Figure 20. Before starting the blockage tests, the three diffraction points, Q_e, Q_e', and Q_e'' are located. Then blockage tests of the lines of sight from the source to Q_e, from Q_e to Q_e', from Q_e' to

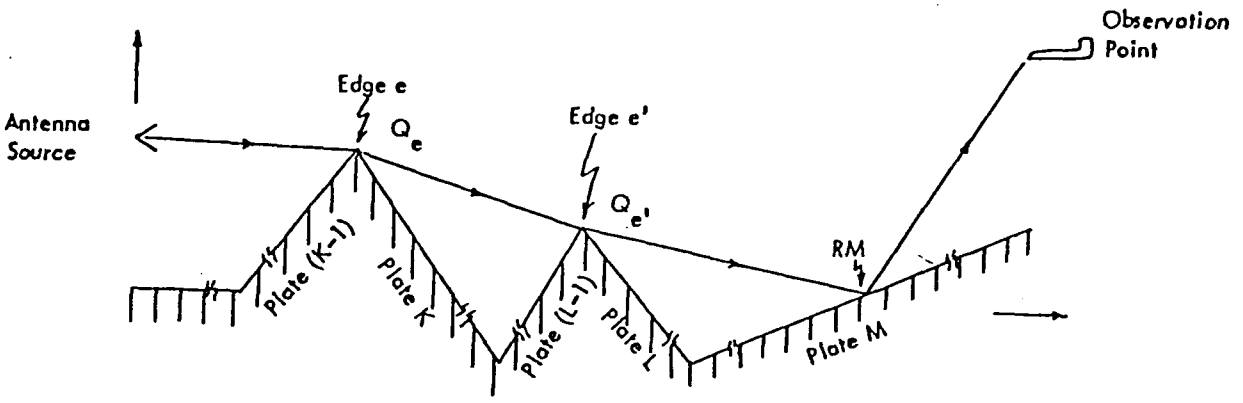

Figure 19. The Diffracted-Diffracted-Reflected Ray Diffracted From Edge e to Edge e′, Diffracted From Edge e′ to Plate M, and Reflected From Plate M to the Observation Point.

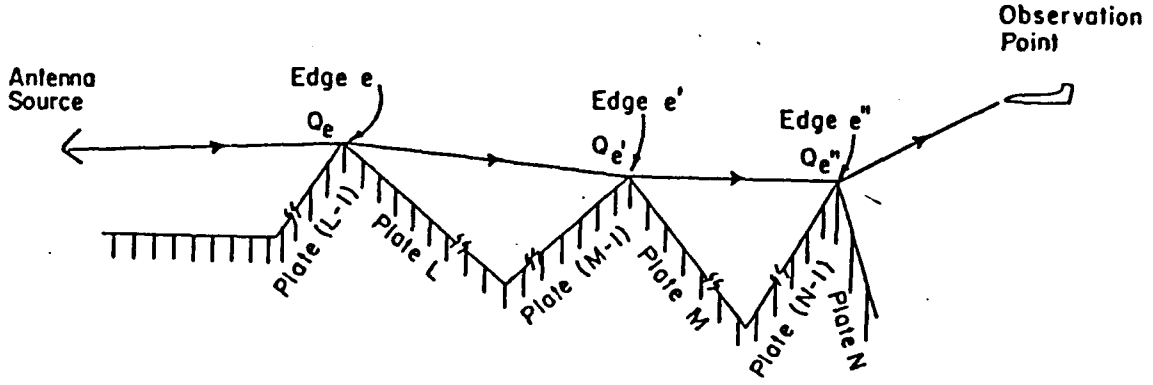

Figure 20. The Diffracted-Diffracted-Diffracted-Ray Diffracted From Edges e, e′, and e″ to the Observation Point.

Q_e'', and from Q_e'' to the observation point are performed. If there is no line of sight blockage, the DDD ray exists and its amplitude is evaluated and added to the sum.

Description of Computer Programs for the Two-Dimensional GTD Model

Most of the two-dimensional GTD model computer subroutines used by Luebbers (1985) are valid and used in this three-dimensional model. In this section we give a brief functional explanation of the

most important subroutines. In the next four sections we describe the revisions and improvements of computer programs for a realistic three-dimensional model of SEL calculation.

Subroutine VGROUN.f

This subroutine VGROUN.f initializes all of the values required for the GTD calculations and acts as a buffer between the main program and the peripheral subroutines.

The observation point and source locations, which are supplied by the main program, are organized for efficient manipulation. Then the normal vector of each plate is determined in such a way that the z-component is negative. The wedge angle, which is formed by two connected plates, is calculated by using their normal vectors and vector cross-product operation. The angle is measured below the terrain profile.

To reduce the calculation time, the lengths in meters are converted to wavelengths. After conversion, subroutines VENGO.f and VETDIF.f determine the relative wave field.

Subroutine VENGO.f

The subroutine VENGO.f calculates the total wave amplitude and phase, which result from the direct, reflected (R), RR, RD, RRD, RDR and RRR rays. The subroutine considers the direct ray first. The direct ray originates from the source and travels directly to the observation point. Subroutine VLOGI1.f checks any possible blockage. If there is no blockage, the direct wave components are calculated by subroutine NWSRCE.f. If the direct ray is blocked, the direct ray contribution is zero.

The reflected rays are considered next. All of the possible singly-reflected rays from every plate are examined within the DO statement 301, where LP is a plate index. When Plate LP is under test, subroutine VEXIST is called to determine the image source (SI) and reflection point OQ on Plate LP. If OQ does exist, the blockage algorithms are started by checking for the blockage from ANT (source point) to OQ, and from OQ to FPTS (observation point). If no blockage occurs (the reflected ray exists), subroutines NWSRCE and FCREFL compute the reflected wave components (ER) from Plate LP. Then ER is added to the total wave (ESUM).

After the reflected ray from Plate LP is evaluated, the doubly-reflected (RR) ray is considered. The DO statement 414 which is looped inside DO statement 301, will examine all of the plates LN that can possibly interact with Plate LP to contribute a RR ray. If LN is equal to LP, no calculation is performed. Plate LN is always located further away from the source than Plate LP. Therefore, only the RR rays traveling in the forward direction are included. The process stops after the last plate (NPLATE) is considered.

Subroutine IMAGE determines a secondary image location (SII) of the image source (SI) with respect to Plate LN. By utilizing pairs (SII, FPTS) and (SI, ANT), two reflection points (OQ, RP) are determined by calling VEXIST twice. OQ and RP must both be located on Plate LN and LP, respectively. If they are not, the RR ray contribution is zero. Also, the lines from ANT to RP, RP to OQ, and OQ to FPTS must not be blocked. If no blockage occurs, routines NWSRCE and FCREFL are called, the RR ray components from Plate LP to Plate LN are determined and then added to ESUM.

During the RR ray determination, several parameters required for the RRD ray calculation are calculated. To save computer time, subroutine VRRD is immediately called for RRD evaluations. The output from subroutine VRRD is added to the total wave field in ESUM.

RD ray contributions are considered next. All possible RD ray contributions from edges are evaluated with DO statement 426. All edges past the edge where plates LP+1 and LP+2 are connected are considered. The RD ray is reflected from Plate LP to the edge and diffracted from the edge to the observation point (FPTS). It should be noted that DO statement 426 is nested within DO statement 301.

The reflection point (RF1) on Plate LP and the possible diffraction point (RP) on Edge LM are calculated first. If both RF1 and RP exist, the blockage algorithms are performed for the blockage from ANT to RF1, RF to RP, and RP to FPTS. If there is no blockage, routine SDDIF is called for evaluation of RD ray amplitude determination. The wave components are determined by routine SDDIF and added to the total field in ESUM.

The remaining rays considered in subroutine VENGO are calculated in separate subroutines called by VENGO. Subroutine VRDR for the RDR rays, subroutine VRDD for both the RDD and RDDD rays, and subroutine VRRR for the RRR rays. The wave components for each ray type are added to the total in array ESUM.

Subroutine VETDIF.f

Subroutine VETDIF.f calculates seven types of rays: Singly-diffracted, DR, DD, DDD, DRD, DDR and DRR rays. It is called only from subroutine VGROUN.

After initialization, the edge formed by two connected plates (LP, LP-1) is considered. With three inputs, the source location, the edge, and the observation point, subroutine VBETA is called for determining the diffraction point (DPT) on the edge. Then, using ANT, DPT, and FPTS, subroutine SDDIF calculates wave components of the singly-diffracted ray. The components are then added to the previous contributions.

The DR ray is considered next, and it must be located on plate LJ. Reflection point C is determined by calling subroutine VEXIST. If either DPT or C do not exist, the DR ray contributions are set to zero, and plate LJ+1 is considered. Otherwise, the blockage algorithm begins by testing the lines from ANT to DPT, from DPT to C, and from C to FPTS. If there is no blockage, the DR ray exists, and subroutine SDDIF determines the ray component.

Following DR ray calculations, DRR rays are examined. This is done by simply calling subroutine VDRR. The wave amplitudes and phases of DRR rays are added to the total.

The next ray to be considered is the DRD ray. If a DRD ray exists, the edge formed by connected plates LR and LR-1, where Plate LR is different from plates LP and LJ, is considered. It should be noted that LR-1 is always greater than LJ. The edge formed by plates LR and LR-1 and FPTS are both imaged with respect to extension of Plate LJ. Using the source location, the edge (formed by plates LP and LP-1), the image of the edge (formed by plates LR and LR-1), and the image of FPTS, the diffraction points DP1 and DP2 are calculated by subroutine V2DIF. If DP1 and DP2 exist, subroutine VEXIST calculates the reflection point location DPT on Plate LJ. If DPT does not lie on Plate LJ, the next edge is considered. Otherwise, the blockage algorithm tests for blockage of the lines from ANT to DP1, from DP1 to DPT, from DPT to DP2, and from DP2 to FPTS. If there is no blockage, subroutine SDDIF is called twice for DRD ray calculations. The ray contributions are added to the total.

The next ray considered in subroutine VETDIF is the DD ray. This ray is diffracted by two edges. The first edge is formed by plates LP and LP-1, whereas the second edge is formed by plates LM and LM-1. Subroutine V2DIF determines two diffraction points (DP1, DP2). The blockage algorithm tests

the lines from ANT to DP1, from DP1 to DP2, and from DP2 to FPTS. If there is no blockage, subroutine SDDIF determines DD ray amplitudes and phases, and they are added to the total.

The next ray considered is the DDR ray. The reflecting plate is LS. The process begins as FPTS is imaged with respect to Plate LS. It is necessary that the image must be located below the plane of Plate LS. Subroutine VEXIST is called to calculate the reflection point C on Plate LS. If C does not exist, the next Plate LS+1 is considered. Otherwise, the blockage is tested on the lines from ANT to DP1, from DP1 to DP2, from DP2 to C, and from C to FPTS. If the lines are not blocked, subroutine SDDIF is called twice for DDR ray amplitude and phase calculations, and the results are added to the corresponding total field components.

Finally, the DDD ray is considered. Blockage and existence tests already performed for the DD ray are used. Since the ray can propagate from edges following plates LP and LM, existence and blockage tests are done from Edge LM to LS and LS to FPTS. If the DDD ray can exist, it is evaluated by calling SDDIF three times and adding the result to the total.

Subroutines VAMPHA.f *and* VAMPH3.f

These subroutines convert real and imaginary components of complex wave fields into amplitudes and phases.

Subroutine VMERGH.f

This subroutine tests for ray blockage when the end points are situated on two consecutive plates, K and L. It is assumed that Plate L is located further away from the source than Plate K.

Subroutine VECTOR.f

This can perform six vector operations, which are: (1) cross product; (2) normalized cross product; (3) unit vector of a difference between two vectors; (4) dot product; (5) projection of two-directional vectors; (6) vector difference between two position vectors.

More detailed descriptions about the subroutines of the two-dimensional GTD model can be found in Luebbers (1985). Documentation and help are also included in the computer programs.

3 THE PROPAGATION MODEL

From Two Dimensions to Three Dimensions

Here the geometrical theory assumption to the reflection of a sound wave by a plate is applied using the same theory for either two- or three-dimensional terrain. However, the diffraction from a hill of finite length is most different from the diffraction of a hill of infinite length in cases where lower-frequency sound waves are used. Although some investigations that extend GTD to lower frequencies could have been used, it was expedient for the present study to continue with the same reflection and diffraction formulae. In this regard, the GTD method itself is somewhat crude, but one of the best models for this situation short of a brute-force numerical procedure.

The amount of diffracted energy re-radiated from an edge is determined by the diffraction coefficient, which is a function of the wedge angle and the incident and diffracted ray geometries. The detailed deduction of formulas used for two-dimensional computations was given by Luebbers for single wedge diffraction. The formulas for double wedge diffraction are given in Chapter 4.

Subroutine VGROUN in the original computer program acts as a buffer between the main GRASS program and the peripheral subroutines. In VGROUN, the x-component of the plates (where the x-axis is parallel to the hills) is extended from −50,000 to 50,000 ft. Normal vectors and wedge angles of the plates are calculated from the four corner positions of each plate. A three-dimensional algorithm was developed to determine the normal vectors and wedge angles of the plates to fit any arbitrarily oriented connected plates. It is therefore more convenient to directly specify the position of the corners as input data to represent the terrain.

The actual calculation of the sound pressure is conducted in the subroutines NWSRCE and SDDIF. Although subroutine VGROUN returns the sound pressure, the sound pressure for each ray is reported by subroutine VAMPH3. Other related subroutines include VENGO, VENDIFF, VRDD, VRDR, VRRD, VMERGH, and VLOGI1. The subroutines were converted or modified for predictions of the sound field in three dimensions above arbitrary three-dimensional terrain. The more complex changes are explained in the following chapters.

Frequency Switch and Blast Waves

The GTD propagation model was used here to calculate the noise levels produced by heavy weapons that generate blast waves. Four parameters are usually used to characterize a blast wave: peak pressure, duration, central frequency, and half-width of the frequency spectrum. For blasts produced by Army weapons, it was necessary to consider a total frequency band from one-third octave band 10 (10 Hz) to one-third octave band 20 (100 Hz). For each one-third octave band, the propagation effects on only the band center frequency were considered. In this way, a wave energy evolution very near that of real, measured waves can be obtained without performing calculations at hundreds of frequencies.

The user may set a switch index (K_f) to choose one of five options for the frequency characteristics of the sound source. When $K_f = 1$, a single frequency source is selected. For single frequency calculations, the user inputs the frequency and the pressure at unit distance (1 m) from the source. When $K_f = 2$, multiple frequencies are used. The user inputs all of these frequencies and the pressure values of the respective frequencies for a specified unit distance from the source. $K_f = 3$ is selected for blast wave calculations. For blast calculations, the user inputs: a maximum pressure (P_{max}); the duration (T_d); the number of frequencies (N_{fre}), the central frequency, and half-width, in response to the prompt by the

program. $K_f = 4$ is also used for blast waves but in this case the user need only input charge and frequency parameters. The computer will calculate the other blast wave parameters P_{max} and T_d from the charge using the following default algorithm:

$$P_{max} = 7.44 \times 10^4 \left(\frac{W}{2.2}\right)^{0.4} \quad \text{[Eq 3]}$$

$$T_d = 3.02 \times 10^{-2} \left(\frac{W}{2.2}\right)^{\frac{1}{3}} \quad \text{[Eq 4]}$$

where the charge weight W is in pounds, P_{max} is the maximum pressure in pascals, and T_d is the duration in seconds. $K_f = 5$ is also used for blast waves, but for this index the only input is the charge size of the weapon. For $K_f = 5$ the computer will not only calculate P_{max} and T_d but also set the frequency range to vary from one-third octave band 10 to one-third octave band 20. Subroutines blast.f and blast1.f calculate the sound pressures at each frequency one unit distance from the explosion.

Noise-Level Weighting Options

Because the sensitivity of the human ear varies with frequency, the significance of noise levels at different frequencies also varies. The International Standard for Sound Level Meters, IEC 651-1979, and its revision, the *American National Standard Institute (ANSI) Specification for Sound Level Meters*, ANSI S1.4-1983, provide a set of A-, B-, C-weighting networks for sound-level meters. As a reference, the revised document also gave similar expressions for the D- and E- weighting networks.

A switch is set in our computer program for the choice of frequency weighting. For the choice $K_w = 0$, no weighting is used. $K_w = 1, 2, 3, 4$, and 5 use A-, B-, C-, D-, and E-weightings, respectively.

4 OTHER PROGRAM IMPROVEMENTS

Subroutine V2DIF determines two diffraction points that exist on two different edges. The arguments included in the original codes included only one diffraction angle. This works when the two edges are parallel, but for three-dimensional terrain, the two edges may not be parallel. Two diffraction angles were set up for the diffractions from the two edges (Figure 21). In the original codes, a plane that includes two edges is introduced as the reference plane. In three dimensions, the two wedges may not necessarily be on one plane. Figure 21 shows A as the source position and F as the observer position. The unit vector u_1 is along the first wedge E_1 - E_2; the unit vector u_2 is along the second wedge E_3 - E_4; Q_1 and Q_2 are two assumed diffraction points. Line AO is perpendicular to u_1 in the plane composed by A and vector u_1. Line Q_2P' is perpendicular to u_1 in the plane composed by Q_2 and u_1. Using single diffraction geometry, the relation between r_1, r_2, r_3, and x_1 is:

$$x_1 = \frac{r_2 \times r_3}{r_1 + r_2} \qquad \text{[Eq 5]}$$

A similar relation exists between r_1, r_2, r_3, and x_2 for a single diffraction of the second wedge.

Therefore, given a source position A and one diffraction point Q_2, another diffraction point Q_1 can be calculated; and given a diffraction point Q_1 and an observation position F, the other diffraction point Q_2 can be obtained. Therefore, given A and F, there are two equations for Q_1 and Q_2, making the calculation of Q_1 and Q_2 feasible. The new subroutine V2DIF uses an iteration method to solve for Q_1 and Q_2. Test runs show the iteration quickly converges with a criteria of one-percent accuracy.

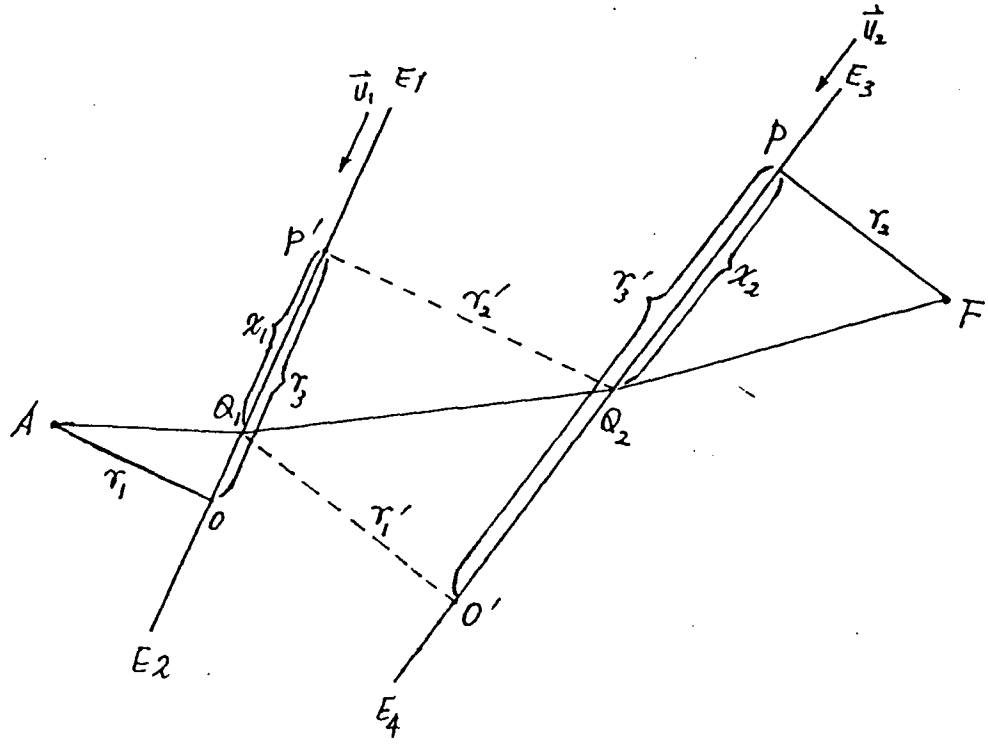

Figure 21. Geometry of Double Diffraction.

The subroutine VMERGH is called when ray blockage occurs where ray end points are situated on two consecutive plates, 1 and 2, and where normal vectors N_1 and N_2 point upward as positive. An alternative method now fulfills this function (Figure 22). If the ray intersects the plates at P_1 and P_2 and the dot product of the vector P_1 to P_2 with N_1 or the vector P_2 to P_1 with N_2 is less than zero, the ray will not be blocked by the valley edge of the two plates. If the dot product is larger than zero, the ray will be blocked by the peak edge of the two plates. This criterion is simpler than the original one, (Houshmand 1990) and the user need not assume that Plate 2 is located farther from the source than Plate 1, as in the original subroutine.

Two bridges were created between "gtd" and "GRASS": a subroutine "tunder.f" was written in Fortran language; and the equivalent function "input.c" was written in C language, and is included as part of this combined program system. Subroutine "tunder.f" is used to find the plates that are under the line connecting the source point and observation point. This subroutine also prepares formatted terrain data on the positions of source, the observation point, and the four corners for each plates.

For accuracy, the subroutine "tunder.f" first distinguishes four different situations according to the observation position with respect to the source point. If the angle between the Source-Observer Line (SOL) and positive x-axis is less than or equal to 45 degrees, the geometrical situation is called a quadrant-1 position. If the angle between the SOL and positive y-axis is less than 45 degrees, the observer is said to be in quadrant 2 with respect to the source. If the angle between the SOL and the negative x-axis is less than or equal to 45 degrees, it is said to be a third-quadrant case. If the angle between the SOL and the negative y-axis is less than 45 degrees, the observer is said to be in the fourth quadrant.

The variable i is used as the row index of the terrain grid cells, and j as the column index (Figure 23). At each grid point, (i,j), GRASS gives the elevation value. Let the bottom-left corner of the terrain be the Cartesian origin (x_0, y_0). The largest row index is "iT." The largest column index is "jT." Figure 23 gives a quadrant 1 situation. Point P is a given source position in the cell with a lower-left corner of A (i_S, j_s). The position (i_s, j_s) is referred to as the source corner. Point F is a given observation position, which is in the cell with a lower-left corner of B (i_o, j_o). We call position (i_o, j_o) the observer corner. Line AB is the SOL. If the intersection point of the SOL and vertical grid line of column index j_c is Q, then the nearest lower corner, G, is called the crossing corner of j_c. The row index of the crossing corner is i_c, making the crossing corner of the source the source corner, and the crossing corner of the observer the

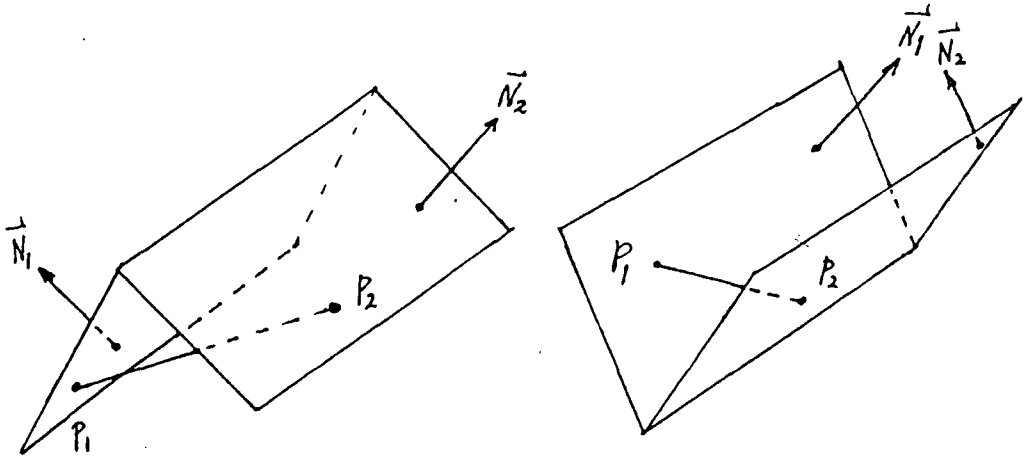

Figure 22. Geometry of Testing Blockage of Ray P1P2 by Wedge.

observer corner. Next determine the bottom corner and top corner. All the column grid lines which cross with the SOL will be the edges of plates. According to our convention, the number of edges are counted from the source to observer corner. Next the bottom corner (i_b, j_b) and top corner (i_t, j_t) of the edges are determined. If the i_c of the farther column grid is larger than the column under consideration, then i_b should be set equal to $i_c + 1$ and the top corner should be set equal to $i_c - 1$. If the i_c of the farther column grid is the same as the present column grid, then set $i_b = i_c$ and $i_t = i_c - 1$. If the farther column has a smaller i_c, the i_b should equal i_c but set $i_t = i_c - 2$. Another principle to determine i_b and i_t is: if the SOL crosses precisely at i_b, increment i_b by 1, i.e., move down one row; if the SOL crosses precisely at i_t, then decrease i_t by 1, i.e., move up one row. This is necessary to avoid shifting the reflection point or diffraction point outside the plate or wedge. The last principle prevents any i from being larger than iT or less than 1, and similarly for j. According to our convention, the corners should be ordered from bottom corner to top corner for the odd edges but from the top to the bottom for the even edges, as demonstrated by the arrows in Figure 23.

Corners c_1, c_2, c_3, and c_4 compose the first plate. Corners c_3, c_4, c_5, and c_6 compose the second plate and so on. Because the elevations of the corners are from terrain data generated by GRASS, it is not guaranteed that the four corners of each plate will lie in one plane. But within the resolution defined here, it is reasonable to force each plate to fit in one plane. The computer "adjusts" the elevation of c_4 to make

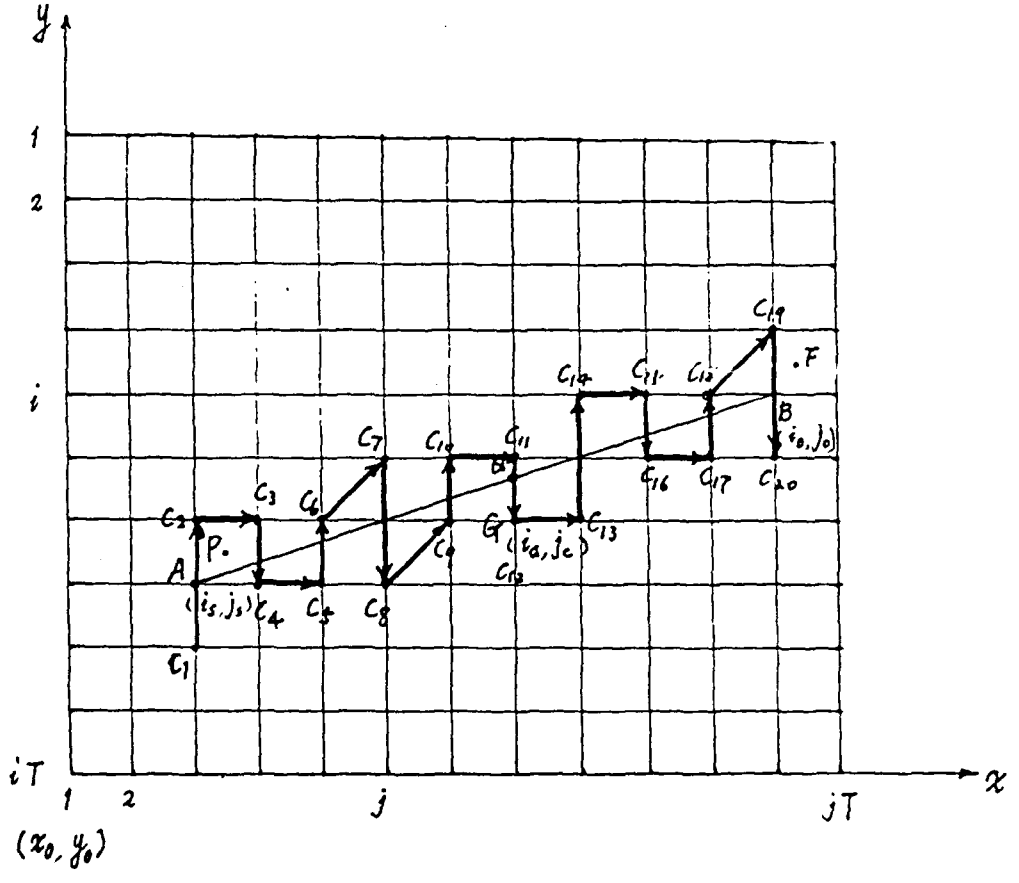

Figure 23. Method of Finding and Rearranging Plates Under the Source-Observer Line.

c_4 into the last corner of the plane of the first plate composed by the corners c_1, c_2, and c_3. The computer "adjusts" the elevation of the last corner of the second plate, c_6, to lie in the plane formed by the adjusted new corner c_4 and the original corners c_3 and c_5 and to assure that the neighboring plates have a common wedge. In this way the elevation of the bottom corners of the even wedges and the top corners of the odd wedges will be adjusted.

By the same reasoning, the computer "adjusts" the elevation of the source position to ensure that the source is situated 2.5 m above the source column (for quadrants 1 and 3) or source row (for quadrants 2 and 4). The computer also "adjusts" the observer's elevation to ensure that the observer is positioned 1.25 m above the observer column (for quadrants 1 and 3) or observer row (for quadrants 2 and 4). The calculations and coordinates are different, but the principles are the same in all four quadrants.

The GTD program uses conventional positions to determine x and y coordinate axes. In quadrant 1, (-y) of the terrain axis is used as (+x) of the "gtd" program axis, and (+x) of the terrain axis as (+y) of the "gtd" axis. In quadrant 2, (+x) of the terrain axis is also taken as (+x) of the "gtd" program axis, and the (+y) of the terrain axis is also taken as (+y) of the "gtd" axis. In quadrant 3, the (+y) direction of the terrain is the (+x) of "gtd" program direction, and the (-x) of terrain will be the (+y) of the "gtd" program axis. In quadrant 4, the (-y) of terrain will be the (+y) of the "gtd" axis, and the (-x) of terrain will be the (+x) of the "gtd" axis.

For the sake of efficiency, the first step is to check neighboring plates to see if they form very small edge angles. If so, they are replaced with larger plates before re-arranging the corner data. For this study, an angle of less than 0.1 radian was set as the small-angle criterion. All of the documented subroutines are listed in the Appendix to this report.

5 THE OVERALL CALCULATION

As mentioned in Chapter 1, terrain data for the calculation of SEL can either be given by the user or input from GRASS output. When the data are given by the user, the computer program will ask the user to input a file name which contains terrain data and then conduct the calculation. Here, conveniently terrain data are supplied by an existing GRASS data base.

To obtain an SEL map as simply as possible, all commands are collected in a profile called "gtdcom," which is saved in (USACERL) directory cerl:/en/usr/zhuang/gtd (Figure 24). Note that directory names are given here only for an example. The user may modify "gtdcom" to specify any directories that contain the programs. A user in a terminal connected to the CERL computer need only type the command "gtdcom" along with the following input parameters:

1. x,y coordinates of the source position
2. Weighting index
3. Charge size in pounds.

Before running "gtdcom," the user must specify the exact terrain data parameters. The terrain data should already be located in a GRASS data base. The geographic region for the terrain data should be correct. The resolution of the cells should be appropriate, i.e., not so fine that the number of cells is too large (usually a region no larger than 50 by 50) and also not so rough that they provide poor accuracy. All these items can be checked by logging in to any GRASS computer, and by using related tools provided in GRASS (Westervelt 1989).

After the computer receives these input parameters, it will follow the procedure shown in Figure 24. The USACERL computer first connects to the computer (zorro) on which GRASS terrain data and programs are stored. This computer will enter the user's GRASS environment, write the geographic region definition parameters to the terrain file "terra.in" as the header, write the raster (cell) elevation data to the terrain file, and remotely copy the terrain file back to the CERL computer and store it in the directory cerl:/en/usr/zhuang/gtd/cases/terra.in for the calculation of "gtd." The CERL computer will disconnect from the other machine and run "gtd." (The group of programs comprising "gtd" is shown in the figure inside the square solid line.) The gtd program will usually take several hours to finish running, depending on the number of cells. One value of the SEL for each cell is calculated by "gtd" computer codes. It takes about 10 seconds for the present CERL computer to compute a single value. The CERL computer will store the SEL data in a file named "final.dat."

After obtaining all the SEL values, the USACERL computer will remotely copy the file "final.dat" to zorro and reconnect to the zorro computer. Then the GRASS tool "r.in.ascii" will be used to convert ASCII "final.dat" file into a binary raster file "final.map." Next, a GRASS tool "p.map" will be used to draw a hardcopy SEL map.

The three main processes of the calculation are to: (1) get terrain data from GRASS, (2) run "gtd" to get SEL values, and (3) display the contour map of SEL. Three by-product files "sumray.dat," "eachry.dat" and "test.dat" may be generated during the calculation of "gtd." The file "sumray.dat" contains more data of each SEL calculation, including the summation of all possible rays (direct ray, reflected rays, and diffracter rays) without weighting for each frequency. The file "eachry.dat" contains the calculated results of sound amplitude without weighting for each ray of sound waves. The file "test.dat" contains necessary debugging data. If the user is interested in obtaining these files, the comments must be cancelled. The two files can be used in checking or examining the numbers in

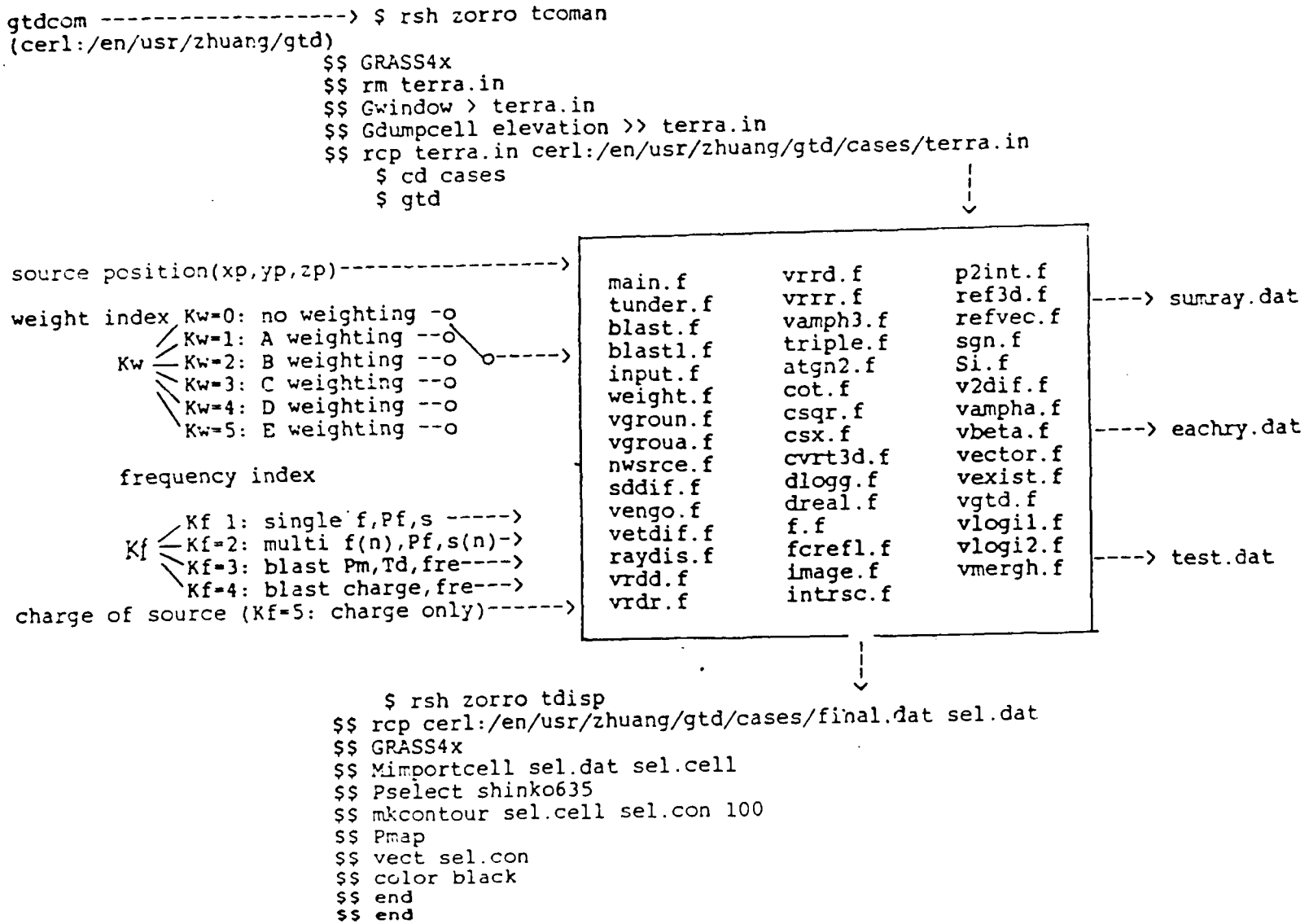

Figure 24. Program Flow Chart.

"final.dat." In the appendix program listing, the subroutine names with extention ".w" are for writing out all results that fill the files "sumray.dat," "eachry.dat," and "test.dat" to standard output.

There are two interfaces between the "gtd" and "GRASS" systems: the interface with the terrain data, and the routine that draws the SEL map. These interfaces correspond with two corresponding commands on the GRASS computer: "tcoman" and "tdisp."

These computer programs implicitly possess the ability to deal with more flexible situations. In addition to the three switches inside the program "main.f" (frequency switch, weighting switch, and ray control index), the user can input arbitrary terrain data by creating the file "terra.in." To do this, the user must delete the commands in the command file "gtdcom" that generate a "terra.in" file.

Even though the "gtd" program sets the maximum number of frequencies to 50, this study used only frequencies from 10 Hz to 100 Hz, to save computer time, and to provide enough range to approximate heavy weapon blast waves. The user may easily change these numbers to fit different purposes.

Pressure is calculated as the summation of the following rays: (1) direct ray, (2) reflected ray, (3) doubly-reflected ray, RR, (4) RD (reflected then diffracted ray), (5) RRD, (6) RDR, (7) D (diffracted ray), (8) DR, (9) DRD, (10) DD, (11) DDR, (12) DDR, (13) RDD, (14) RRR, (15) DDD, (16) RDDD. These 16 numbers determine whether to include or exclude the relevant ray. If a number's value is zero, the relevant ray will be included, but if a number's value is 1, the relevant ray will be excluded. Because the triple diffraction ray is usually very weak, and because it was necessary to save computer time, rays 15 and 16, which have DDD rays, were simply dropped. In the final version of programs for this study, all other 14 ray indexes were set to zero.

6 TWO SAMPLE RUNS

The GRASS data file "Pinyon" shows typical terrain features at Pinyon Canyon, CO. Figure 25 shows sample elevation data, smoothed from the original 50-meter resolution geographical data. Before running the programs, the terrain data need some preparation:

1. Enter the GRASS environment and choose "mapset pinyon"

2. Use the GRASS tool "r.neighbors" to smooth the elevation data

3. Use the "g.region tool to set resolution = 4000 (meters), and the east-west-north-south boundaries. The job may now be run, as explained in the previous section. Figure 25 shows the contents of the intermediate file "terra.in." The format of file "terra.in" is specified by "gtd" programs. The first four lines give the boundary coordinates of the terrain area considered. The fifth line gives the total row number "*i*T." The sixth line is the total column number "*j*T." The matrix takes the form *i*T by *j*T, which gives the elevation of each pixel in the area. Therefore, the first line of the matrix is for row 1, column 1, 2, 3 . . . *j*T.

Figure 26 shows the contour map of elevations of the terrain in the area described in Figure 25. The upper left corner is the highest region, and the bottom right corner is the second highest hill. The lowest place is located in the upper right corner. Figure 27 shows the contour map of a calculated SEL, the final result generated by "gtd" and GRASS. The maps shown in Figures 26 and 27 use the same region and grid size. The SEL mapped in Figure 27 is from a 1-lb (0.453 kg) explosive source at the center cell. The "final.dat" file contents are shown in Figure 28.

SEL field measurements were taken at the Fort Leonard Wood, MO training site in 1989. Elevation data are not available for this region in a GRASS data base. Table 2 gives estimated elevation data taken

```
north:      4159950
south:      4127950
east:       609950
west:       569950
rows:       8
cols:       10
206 202 191 185 172 160 137 124 114 113
208 205 195 186 170 157 135 124 114 112
207 206 198 185 162 148 130 121 114 112
201 200 191 178 155 142 128 122 117 116
188 187 178 168 149 138 128 126 129 130
182 181 173 164 147 138 132 133 140 143
176 175 168 160 146 141 141 146 156 159
175 173 166 158 146 142 144 151 161 164
```

Figure 25. Sample Grid Cell Elevation Values at Pinyon Canyon, CO

window: **north: 4159950 m**
south: 4127950 m
west: 569950 m
east: 699950 m
grid size: 40km × 40km

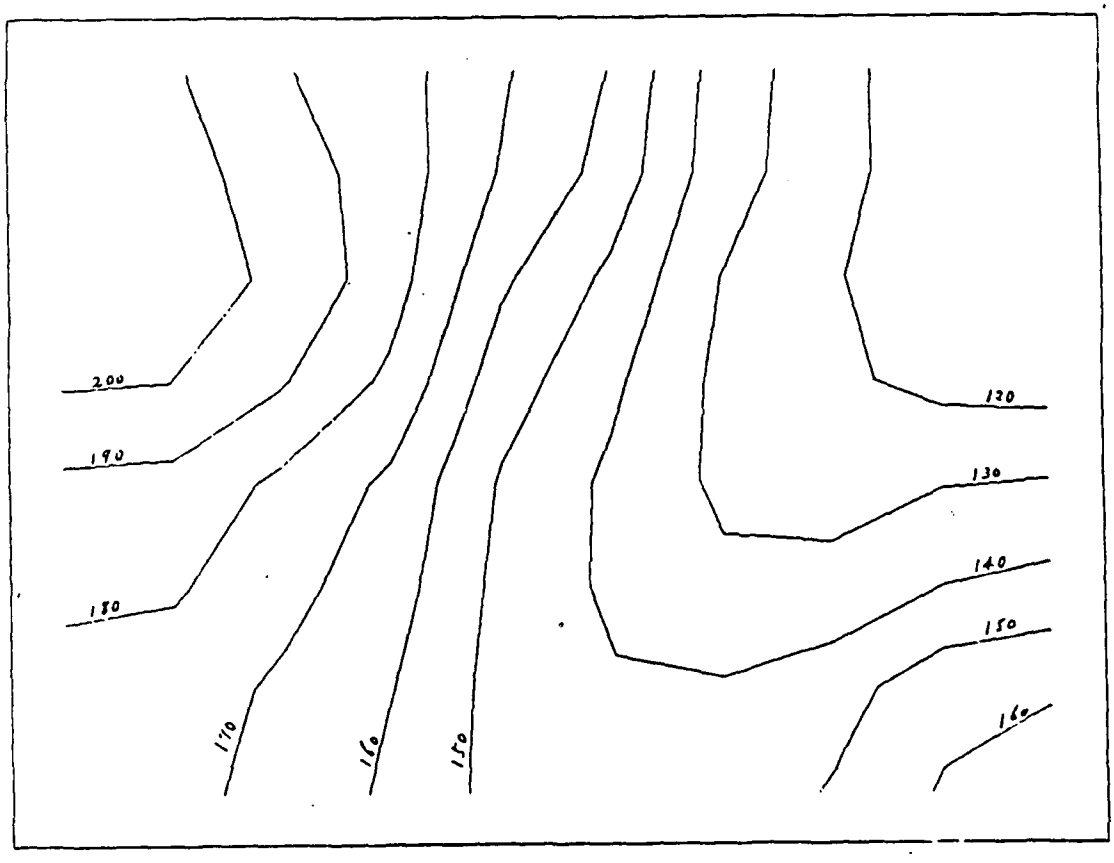

Figure 26. Elevation Contours in the Pinyon Canyon Region.

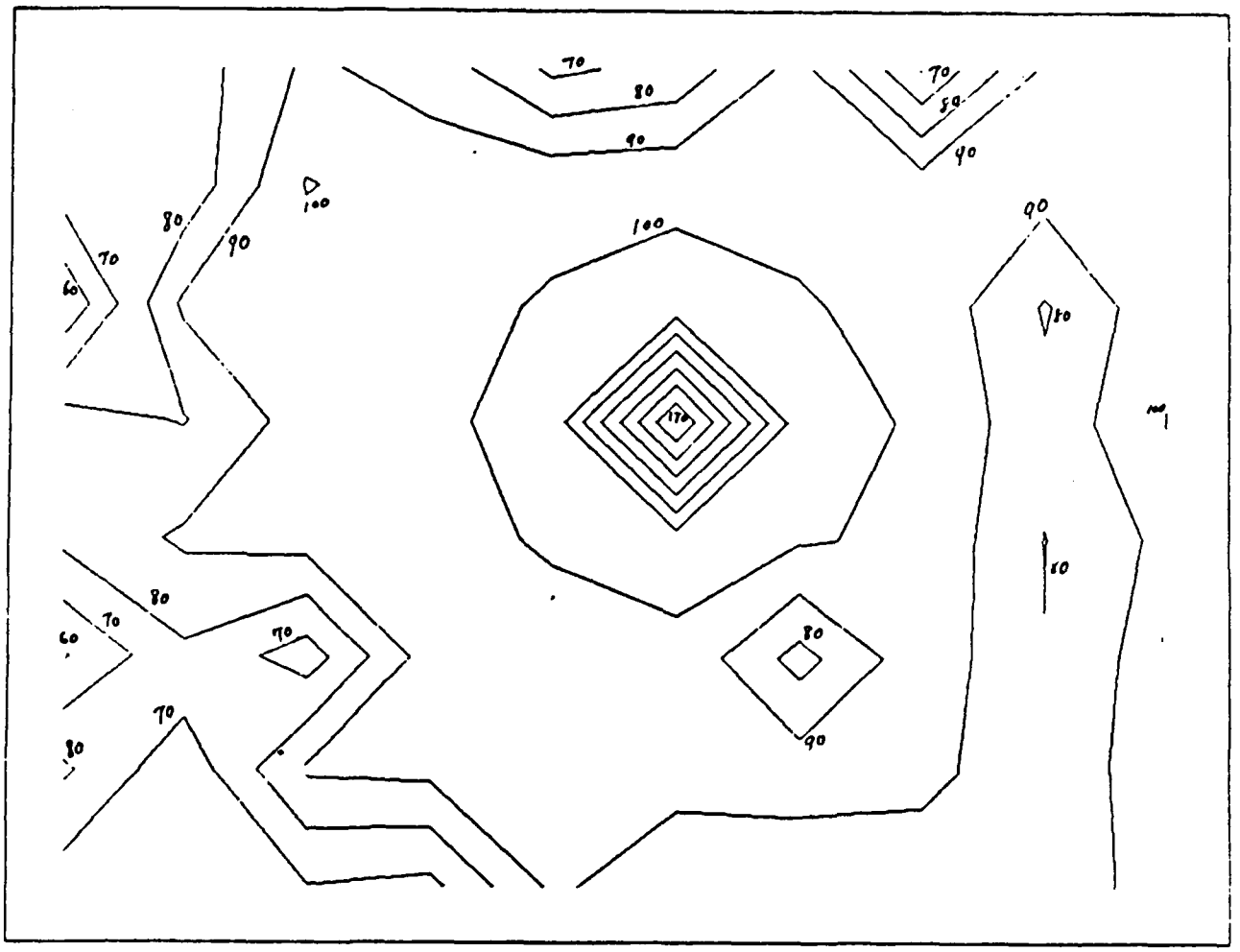

Figure 27. Contour Map of Calculated SEL Values for Pinyon Canyon, CO.

by hand from a contour map. Table 3 lists the positions of two blast sources and seven microphones. Tables 4 and 5 give calculated SEL values for the training site, for a grid size of 1000 m. Figures 29 and 30 respectively show elevation contours based on Table 2 and the calculated SEL based on Tables 4 and 5. Both Figures 29 and 30 are based on the following parameters: (1) region: north 78500m; south 72500m; east 86500m; west 68500m, (2) grid size: 100m x 100m. Figure 29 was derived from information taken from blast 1, and Figure 30 from blast 2. Table 6 lists observed SEL data, averaged from original measured data. The numbers in the parentheses are root mean square errors. The calculated values are the SEL values multiplied by 10, to create three-digit measurements, and to meet the GRASS requirement that data for map drawing be integers. A comparison between Tables 4 and 5 with 6 and 7 shows some agreement between calculated and observed SEL variation and distance. In general, the calculated values are larger than the measurements. This is probably because the dissipation of the atmosphere and the roughness of the ground were not included in the model. In addition, other errors may have arisen from the elevation estimation and the large grid size.

We have chosen the above two sites because they represent, in our opinion, extreme examples of the kind of terrain that may be encountered at Army bases around the world. Fort Leonard Wood site has very large variations in altitude from place to place. It is typical of the terrain in Germany where there are highly visible noise problems.

north: 4159950.0000000
south: 4127950.0000000
east: 609950.0000000
west: 569950.0000000
rows: 8
cols: 10

785	739	916	864	681	729	940	598	920	905
762	725	1006	949	970	979	970	949	932	967
518	918	941	973	1009	1040	1009	970	790	971
837	794	946	979	1040	1705	1040	989	830	1003
825	916	941	975	1009	1040	1009	981	797	925
590	780	648	950	969	978	763	966	802	964
818	633	913	926	944	951	954	938	811	979
653	617	699	675	921	811	823	825	812	968

Figure 28. Sample Grid Cell Values (×10) for Calculated SELs in the Pinyon Canyon Region.

Table 2

Estimated Elevation Data for Fort Leonard Wood Region

(From sheet 7559 II Series v 779 Ed 6-DMA taken from 10 m contour lines on kilometer grid scale 1:50000)

N, E		N, E		N, E		N, E		N, E		N, E	
(78,69)	265	(77,69)	300	(76,69)	320	(75,69)	310	(74,69)	340	(73,69)	290
(78,70)	300	(77,70)	322	(76,70)	330	(75,70)	350	(74,70)	340	(73,70)	305
(78,71)	310	(77,71)	320	(76,71)	345	(75,71)	345	(74,71)	340	(73,71)	360
(78,72)	280	(77,72)	300	(76,72)	328	(75,72)	310	(74,72)	330	(73,72)	340
(78,73)	325	(77,73)	325	(76,73)	305	(75,73)	310	(74,73)	335	(73,73)	348
(78,74)	260	(77,74)	340	(76,74)	333	(75,74)	325	(74,74)	325	(73,74)	338
(78,75)	330	(77,75)	340	(76,75)	342	(75,75)	345	(74,75)	342	(73,75)	335
(78,76)	325	(77,76)	350	(76,76)	345	(75,76)	340	(74,76)	343	(73,76)	338
(78,77)	340	(77,77)	350	(76,77)	340	(75,77)	320	(74,77)	320	(73,77)	315
(78,78)	330	(77,78)	340	(76,78)	330	(75,78)	335	(74,78)	320	(73,78)	333
(78,79)	330	(77,79)	315	(76,79)	300	(75,79)	285	(74,79)	305	(73,79)	310
(78,80)	330	(77,80)	300	(76,80)	260	(75,80)	260	(74,80)	290	(73,80)	320
(78,81)	300	(77,81)	260	(76,81)	240	(75,81)	300	(74,81)	290	(73,81)	330
(78,82)	300	(77,82)	240	(76,82)	315	(75,82)	245	(74,82)	285	(73,82)	250
(78,83)	310	(77,83)	260	(76,83)	250	(75,83)	245	(74,83)	240	(73,83)	260
(78,84)	235	(77,84)	240	(76,84)	270	(75,84)	285	(74,84)	245	(73,84)	300
(78,85)	320	(77,85)	310	(76,85)	310	(75,85)	335	(74,85)	320	(73,85)	330
(78,86)	250	(77,86)	285	(76,86)	285	(75,86)	320	(74,86)	320	(73,86)	340

Table 3

Position of Two Blast Sources and Seven Microphones

Blast 1	84.68 Km,	77.48Km,	291.10 m
Microphone1	84.68	77.18	289.74
Microphone2	82.20	77.46	271.88
Microphone3	79.25	76.60	303.95
Microphone4	76.78	75.46	333.28
Microphone5	74.54	74.67	336.47
Microphone6	71.95	74.58	320.83
Microphone7	69.81	73.71	330.22
Blast 2	69.28	73.83	333.21

Table 4

Calculated SELs Generated by Blast 1 at Fort Leonard Wood

Blast 1, generated by at 84.68 km, 77.48 km

Window:	north:	78500.0 m
	south.	72500.0 m
	east:	86500.0 m
	west:	68500.0 m
	grid size:	1000.00 m
	rows:	6
	cols:	18

No-weighting, 1-lb charge

700	749849	709	702	890	790	980	844	1040	1007	1036	957	858	1073	1048	1078	1048
696	605807	621	744	590	847	737	924	902	931	694	807	1070	1078	1078	1627	1078
759	620807	758	705	832	967	975	830	992	908	919	778	1000	1032	1048	1078	1048
858	703865	838	717	426	716	988	800	1011	1018	1025	974	1017	823	856	1079	1067
587	802822	871	675	778	811	991	840	1021	889	1017	997	975	638	878	889	853
701	792924	924	826	868	789	888	831	954	879	976	979	727	864	680	949	915

No-weighting, 5-lb charge

792	829920	782	781	974	873	1063	931	1124	1084	1119	1036	949	1157	1130	1160	1130
784	699888	711	840	694	915	810	1000	984	1016	768	890	1153	1152	1160	1705	1160
848	718890	833	798	908	1051	1059	906	1069	1009	1006	863	1067	1109	1130	1160	1130
942	782946	944	818	494	778	1069	884	1082	1084	1096	1054	1092	897	939	1153	1142
665	893923	944	755	853	885	1073	926	1107	984	1098	1074	1052	712	957	974	945
806	887011	1019	906	963	889	985	918	1025	961	1051	1053	831	924	754	1032	1005

c-weighting, 1-lb charge

673	728830	689	679	867	767	957	819	1017	988	1015	936	831	1050	1027	1057	1027
671	576786	594	714	556	830	719	906	881	908	676	785	1048	1060	1057	1610	1057
735	589784	743	682	809	944	953	811	973	874	895	753	985	1012	1027	1057	1027
835	682844	801	683	410	702	968	779	993	1003	1007	954	999	805	833	1061	1049
566	775789	852	652	759	789	968	817	997	861	996	977	956	620	858	865	826
667	766902	896	806	838	758	858	808	937	856	957	961	693	852	662	926	889

c-weighting, 5-lb charge

752	790888	752	744	936	828	1024	890	1085	1051	1081	1001	903	1119	1092	1122	1092
741	651852	666	789	639	888	781	967	946	976	737	851	1114	1121	1122	1673	1122
805	667852	803	757	875	1011	1020	873	1036	952	964	820	1043	1075	1092	1122	1092
903	747910	886	765	468	756	1032	845	1053	1061	1067	1018	1060	866	900	1122	1110
630	851878	911	716	820	850	1035	884	1066	934	1060	1040	1018	681	922	933	899
757	844970	973	860	913	833	935	875	995	923	1019	1022	774	906	723	993	960

Table 5

Calculated SELs Generated by Blast 2 at Fort Leonard Wood

window:	north:	78500.0 m
	south:	72500.0 m
	east:	86500.0 m
	west:	68500.0 m
	grid size:	1000.0 m
	rows:	6
	cols:	18

No-weighting, 1-pound charge

871	952	500	1039	907	700	909	701	901	652	709	768	677	680	704	718	698	704
888	889	878	817	922	717	922	567	826	500	500	726	500	765	500	500	711	500
963	1063	1029	850	927	883	864	574	728	703	500	749	657	657	656	720	724	681
1018	1048	1027	832	824	698	816	765	545	624	500	524	500	657	500	496	707	500
1627	1078	830	794	833	808	708	836	671	806	622	741	500	500	500	710	775	808
1018	1048	817	810	823	704	783	770	692	742	734	651	738	656	632	624	726	661

No-weighting, 5-pound charge

948	1033	500	1123	996	786	999	794	989	749	803	858	777	775	799	794	791	799
967	972	961	911	1011	808	1015	682	916	500	500	828	500	865	500	500	814	500
1033	1138	1104	941	1016	967	949	676	821	797	500	846	745	744	741	814	808	784
1100	1130	1106	911	916	793	911	845	654	734	500	610	500	751	500	583	787	500
1705	1160	901	887	920	896	793	926	763	896	721	832	500	500	500	801	863	897
1100	1130	887	899	909	793	875	851	777	829	813	738	838	752	736	707	834	757

C-weighting, 1-pound charge

853	930	500	1017	882	675	883	677	876	622	681	742	644	651	674	699	671	674
686	866	855	789	897	688	893	525	800	500	500	693	500	732	500	500	679	500
948	1045	1010	824	901	860	840	549	700	675	500	720	632	632	633	694	703	650
997	1027	1007	812	797	670	788	743	509	587	500	500	500	629	500	471	686	500
1610	1057	813	766	809	783	684	809	643	781	590	715	500	500	500	683	750	782
997	1027	800	785	799	678	758	749	666	718	715	626	707	625	598	603	685	632

C-weighting, 5-pound charge

915	996	500	1983	952	740	955	745	946	700	756	810	723	728	751	760	748	748
931	933	922	863	968	764	966	617	871	500	500	770	500	817	500	500	763	500
1006	1106	1072	896	972	928	908	623	774	749	500	796	702	702	700	765	768	732
1062	1092	1071	876	870	744	862	809	594	672	500	569	500	703	500	541	749	500
1673	1122	873	840	878	853	753	881	717	852	669	787	500	500	500	755	820	853
1062	1092	860	856	868	749	834	812	735	786	779	696	788	705	682	666	779	712

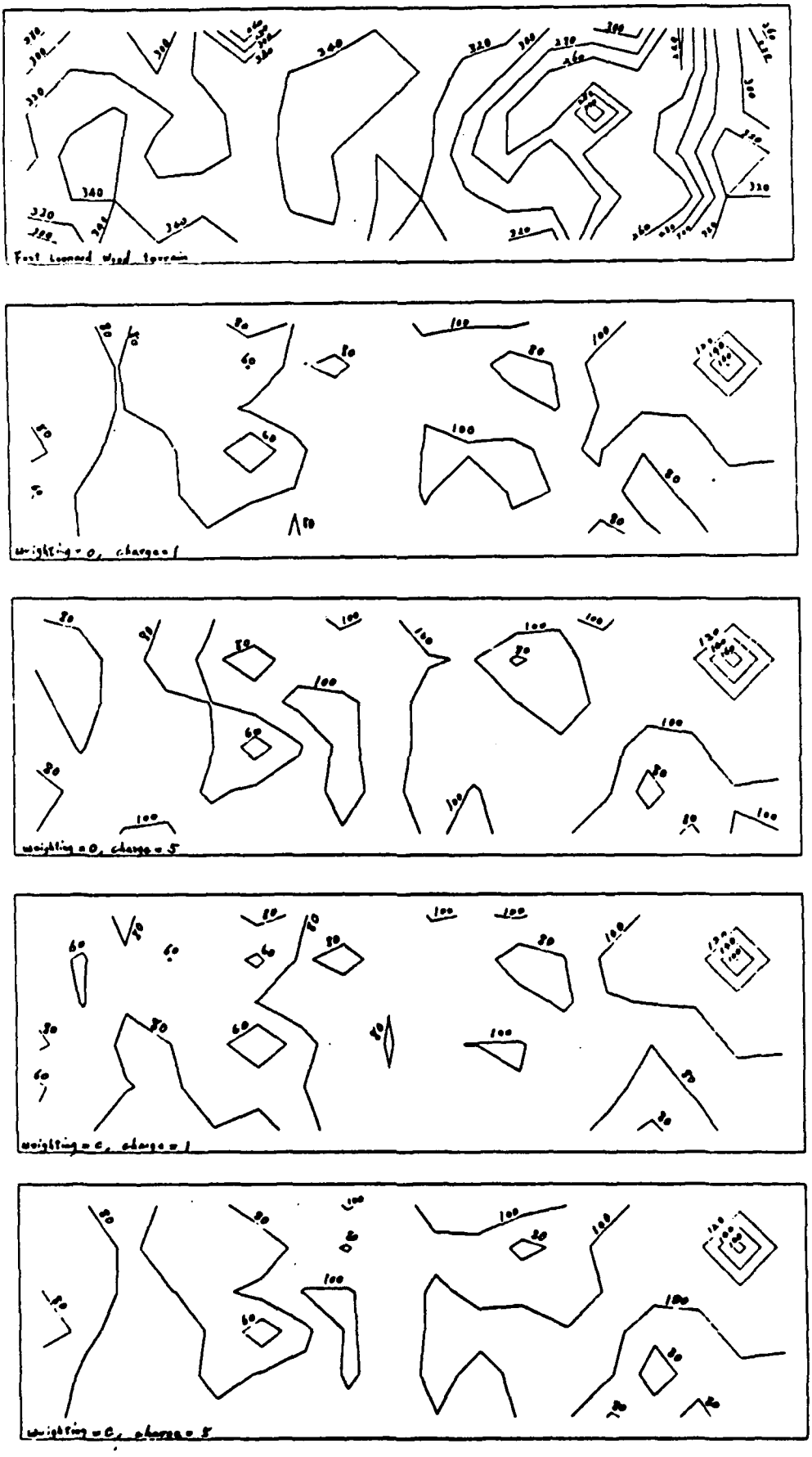

Figure 29. Elevation Contours in Fort Leonard Wood, MO, Region.

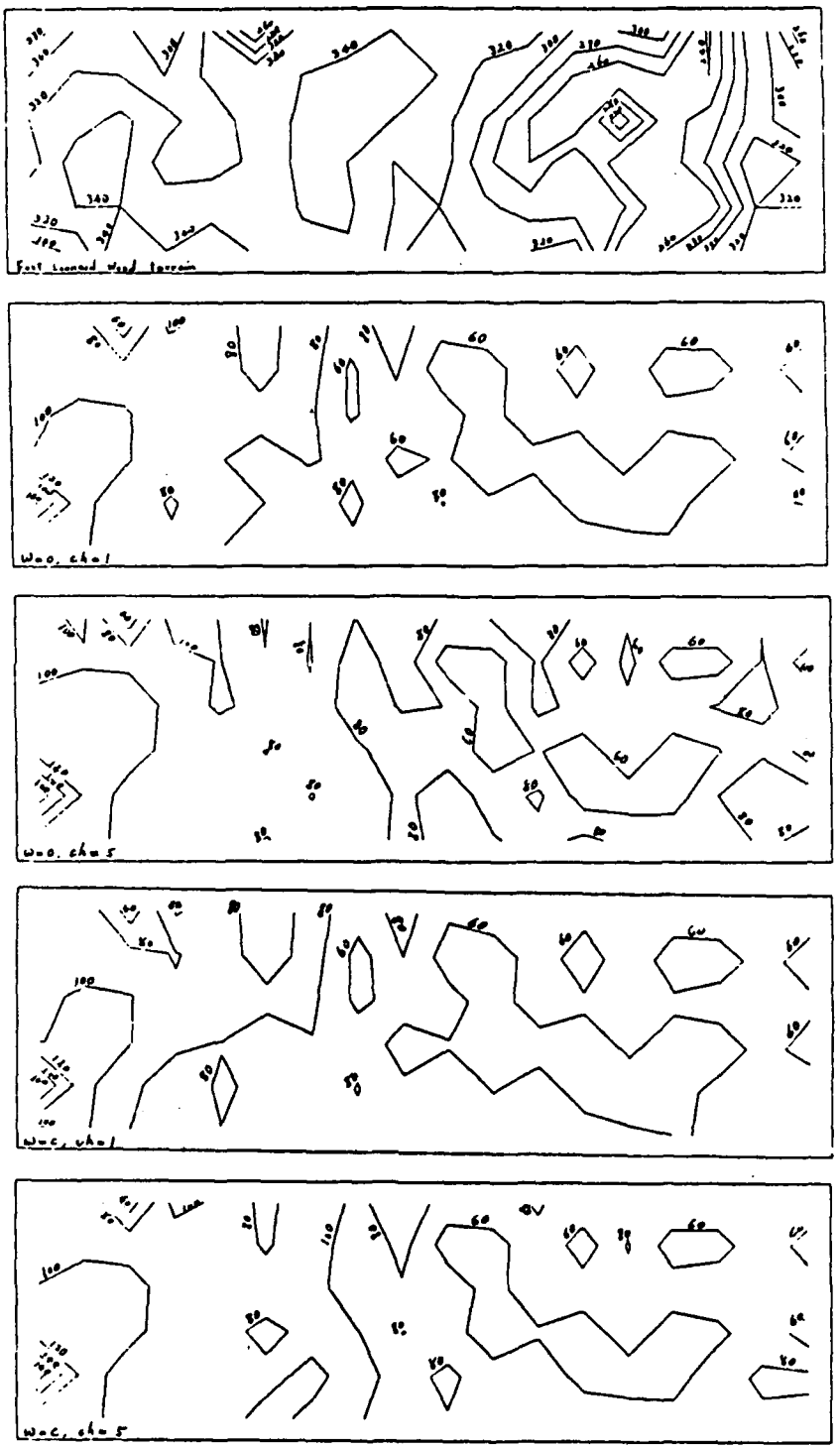

Figure 30. Contours of Calculated SEL in Fort Leonard Wood Region.

Table 6

Average Values and Mean Square Errors of SEL Measurements

Blast Site	1		1		2		2	
Wt. Index	0		3		0		3	
Charge Size	1	5	1	5	1	5	1	5
Mic. 1	115.7 (1.2)	121.9 (1.5)	113.0 (1.2)	117.9 (1.5)	272.5 (7.4)	79.0 (7.4)	67.3 (7.9)	71.0 (9.4)
Mic. 2	79.2 (7.2)	87.4 (6.5)	73.9 (8.6)	80.1 (8.1)	69.7 (8.4)	77.0 (8.8)	64.8 (9.2)	69.8 (10.1)
Mic. 3	68.6 (7.7)	76.6 (8.5)	63.4 (8.7)	67.7 (9.8)	71.2 (7.3)	79.7 (7.0)	65.5 (8.4)	71.1 (8.2)
Mic. 4	70.3 (7.1)	76.8 (8.8)	65.4 (7.5)	69.8 (9.8)	76.2 (6.1)	84.1 (6.5)	70.1 (7.1)	75.2 (7.0)
Mic. 5	68.8 (7.3)	75.8 (7.7)	64.8 (7.7)	69.1 (8.9)	77.6 (6.5)	87.2 (5.4)	71.3 (7.5)	78.9 (6.0)
Mic. 6	67.2 (6.8)	72.9 (8.3)	62.9 (7.0)	66.2 (8.4)	86.7 (6.6)	95.0 (6.7)	81.4 (7.0)	87.4 (7.2)
Mic. 7	66.9 (7.8)	73.1 (8.9)	62.5 (8.5)	66.1 (9.6)	107.6 (2.6)	114.6 (2.5)	104.0 (2.5)	110.0 (2.3)

7 SUMMARY

This report describes a GTD propagation model that approximates acoustic wave propagation over hills and realistic terrain. The realistic terrain data can be either input by the user or supplied by a GRASS geographic information system data base. The calculation is basically a point-to-point calculation. When the terrain data are input by the user and one observation point is considered, the computation is straightforward and very quick. The user can obtain not only the total sound level, but also the components of the sound levels generated by different mechanisms, e.g., directly propagated from source to the receiver; reflected from the ground surface; diffracted from hill edges and so on.

The GTD model was interfaced with GRASS programs to predict the SEL for an explosive source above a specified terrain. The modified system calculates SEL's for the defined area to produce an SEL map. Sample runs on data from the Pinyon Canyon, CO and the Fort Leonard Wood, MO regions were described. The final version of the program was designed for simplicity. The user supplies a source position, charge size, and an expected weighting, and then the computer calculates the SEL for each grid cell of a given terrain area, and creates a contour map for the SEL in this area. For this study, GRASS programs were altered so that the user need only type "gtdcom" to begin the program, and then follow a series of screen prompts to enter a noise-weighting index (A to E) and an effective charge weight in pounds. As the program calculates, the SEL results for each cell of the terrain are displayed on the screen, so that the user may monitor the process. After all cell calculations are completed, a hard copy of the contour map of SEL values is prepared and sent to a printer.

Comparison of the calculated SEL values and the contour maps with the observed data shows a tendency for agreement between the variation of observed SEL with distance, and (theoretical) SEL predictions.

The program calculations used in this study were based on ray acoustic theory. The application of ray theory to sound waves is an approximation, especially at very low frequencies. For this reason, high accuracy is of little importance for the other aspects of the calculation. For example, the diffraction theory for a infinite edge was used in the situation with a finite edge for three-dimensional terrain. At most, doubly-diffracted rays were included; triple diffraction rays, and so on were excluded. Although we found it feasible to apply geometric ray theory to sound wave propagation over realistic terrain, much improvement would be expected if the calculation were based on wave theory instead of the approximations inherent in geometric ray theory.

The original gtd program required that terrain data be supplied in such a way that consecutive pairs of points formed parallel lines. This requirement set a strong constraint on the calculation, with unavoidable implications. The present procedure calculates diffraction and reflection simultaneously. This procedure may not be best when applying geometric ray theory in three dimensions. A possible alternative might be first to find the hills (edges) and planes for the terrain area, then to calculate diffraction rays and reflected rays, and finally to sum them up to get SEL values. The proposed alternate method may save computer time and avoid losing rays from any plates and edges in the considered area. One way to achieve this would be to carefully select diffraction edges from a given terrain to reduce the number of edges considered and to include all possible rays. Only important edges would be used as diffraction edges, rather than every cell boundary under the SOL in the map.

This study revealed several sources of error in calculation that are expected to be reduced in future work:

1. To save computer time and maintain accuracy, only the terrain effects under the direct path from the source to the observation point were considered. This study ignored the terrain effects in the backward direction from the source-observation line. If the source and observation lie in a valley, the reflection ray from the side plates may be significant. It would not be very difficult to include the effects from the side plates and the back plates, but this was not done in this development.

2. The sound waves produced by a heavy weapon may propagate over several kilometers. To find out the SEL for the whole affected region, the resolution of terrain cells should not be so fine that the number of cells is consequently very large. To model the effects of fine structure near the source on the noise level, the cell size should be set relatively small to obtain the SEL map for a small area. However, the accuracy of SEL results for a finer resolution is not necessarily higher than a rough resolution. Furthermore, the resolution should be set in relation to the region of terrain area. The gtd programs demand the same resolution for both x and y coordinates, while GRASS may supply different resolutions for x and y coordinates, i.e., the east-west and north-south directions. To avoid this possible discrepancy, the user should ensure that the resolution and the sizes of the terrain area in both x and y directions are the same.

REFERENCES

Chamberlin, K., and R.J. Luebbers, "An Evaluation of Longley-Rice and GTD Propagation Models," *IEEE Transactions on Antennas and Propagation*, Vol AP-30 (November 1982), p 1093.

Keller, J.B., "Geometrical Theory of Diffraction," *J. Opt. Soc. Amer.* (1962), pp 116-130.

Kouyoumjian, R.G., and P.H. Pathak, "A Uniform Geometrical Theory of Diffraction for an Edge in a Perfectly Conducting Surface," *Proc. IEEE* (November 1974), pp 1448-1461.

Houshmand, B., et al., *GTD Propogation Model for Acoustic Propogation Over Hills and Ridges* (Department of Electrical and Computer Engineering, University of Illinois, Urbana, January 1990).

Luebbers, R., V. Ungvichian, and L. Mitchell, "GTD Terrain Reflection Model Applied to ILS Glide Slope," *IEEE Trans. Aerosp. Electron. Syst.*, Vol AES-18 (January 1982), p 11.

Pierce, A.D., *Acoustics: An Introduction to Its Physical Principles and Applications* (Acoustical Society of America, NY, 1989).

Rojas-Teran, R.G., and W.D. Burnside, *GTD Analysis of Airborne Antennas in the Presence of Lossy Dielectric Layers*, Report No. 710964-8 (Ohio State University Electro-Science Laboratory, August 1981).

Westervelt, James, et al., *GRASS User's Reference Manual*, Automatic Data Processing (ADP) Report N-87/22 (U.S. Army Construction Engineering Research Laboratory [USACERL], November 1989).

APPENDIX: Program Listing

* Modified subroutine.
** Newly created subroutine.
*** Deleted subroutine.

DISTRIBUTION

Chief of Engineers
ATTN: CEHEC-IM-LH (2)
ATTN: CEHEC-IM-LP (2)
ATTN: CERD-L

Ft. Belvoir, VA 22060
ATTN: CECC-R

Defense Technical Info. Center 22304
ATTN: DTIC-FAB (2)

8
11/92

☆ U.S. GOVERNMENT PRINTING OFFICE: 1993 — 3510-S\80017